COPERNICUS SPACE COMPONENT SENTINEL OPTICAL IMAGING

MISSION PERFORMANCE CLUSTER SERVICE

Data Quality Report

Sentinel-3 SLSTR - October 2023

Ref.: OMPC.LDO.DQR.04.10-2023
Issue: 1.0
Date: 10/11/2023
Contract: 4000136252/21/I-BG

Customer:	ESA	**Document Ref.:**	OMPC.LDO.DQR.04.10 -2023
Contract No.:	4000136252/21/I-BG	**Date:**	10/11/2023
		Issue:	1.0

Project:	COPERNICUS SPACE COMPONENT SENTINEL OPTICAL IMAGING MISSION PERFORMANCE CLUSTER SERVICE		
Title:	Data Quality Report - SLSTR - October 2023		
Author(s):	SLSTR ESL team		
Approved by:	P. Paolino, OPT-MPC SLSTR ESL Coordinator	**Authorized by**	C. Henocq, OPT-MPC S3 Technical Manager
Distribution:	ESA, EUMETSAT, published in Sentinel Online		
Accepted by ESA	S. Dransfeld, ESA TO		
Filename	OMPC.LDO.DQR.04.10-2023 - i1r0 - SLSTR Data Quality Report October 2023.docx		

Disclaimer

The views expressed herein can in no way be taken to reflect the official opinion of the European Space Agency or the European Union.

Changes Log

Version	Date	Changes
1.0	10/11/2023	First version

Table of content

1 EXECUTIVE SUMMARY 1

2 PROCESSING STATUS 3

2.1 PROCESSING BASELINE STATUS 3
2.2 PROCESSING ANOMALIES 4

3 EVENTS AND INSTRUMENT ANOMALIES 5

3.1 SLSTR-A 5
3.2 SLSTR-B 5

4 INSTRUMENT STATUS 6

4.1 INSTRUMENT TEMPERATURES 7
4.1.1 SLSTR-A 7
4.1.2 SLSTR-B 8
4.2 DETECTOR TEMPERATURES 9
4.2.1 SLSTR-A 9
4.2.2 SLSTR-B 10
4.3 SCANNER PERFORMANCE 11
4.3.1 SLSTR-A 11
4.3.2 SLSTR-B 12
4.4 BLACK-BODIES 13
4.4.1 SLSTR-A 14
4.4.2 SLSTR-B 15
4.5 DETECTOR NOISE LEVELS 16
4.5.1 SLSTR-A VIS and SWIR channel signal-to-noise 16
4.5.2 SLSTR-B VIS and SWIR channel signal-to-noise 19
4.5.3 SLSTR-A TIR channel NEDT 21
4.5.4 SLSTR-B TIR channel NEDT 23
4.6 CALIBRATION FACTORS 26
4.6.1 VIS and SWIR radiometric response 26
4.6.2 SLSTR-A 26
4.6.3 SLSTR-B 28

5 LEVEL-1 PRODUCT VALIDATION 31

5.1 LEVEL-1 TIR RADIOMETRIC VALIDATION 31
5.2 LEVEL- 1 VIS SWIR RADIOMETRIC VALIDATION 31
5.2.1 Radiometric validation with DIMITRI 32
5.3 LEVEL-1 GEOMETRIC VALIDATION 40
5.3.1 SLSTR-A 41
5.3.2 SLSTR-B 42

6 LEVEL 2 LST VALIDATION 43

6.1 CATEGORY-A VALIDATION 43
6.2 CATEGORY-C VALIDATION 48
6.3 LEVEL-3C ASSESSMENT 50
6.4 REFERENCES 50

7 LEVEL 2 FRP VALIDATION 52

7.1 THE SLSTR FIRE RADIATIVE POWER PRODUCT 52
7.2 VALIDATION METHODOLOGY 52
7.3 RESULTS 54
7.3.1 Global distributions of the fires 54
7.3.2 Nighttime Fires Validation 55
7.3.3 Daytime Fires Validation 57
7.3.4 Biome influence on active fire detection 59
7.4 CONCLUSION 60

8 APPENDIX A 61

List of Figures

Figure 1: OME temperature trends for SLSTR-A (left) and Baffle temperature trends (right) during October 2023. The OME plot shows the three paraboloid stops and flip baffle (top two plots) and optical bench at different positions (third plots), and scanner and flip assembly (bottom plots). The Baffle plot shows the temperature at different positions on the inner and outer baffles. Each dot represents the average temperature in one orbit. ---------- 7

Figure 2: SLSTR-B OME temperature trends (left) and Baffle temperature trends (right) during October 2023. The OME plot shows the three paraboloid stops and flip baffle (top two plots) and optical bench at different positions (third plots), and scanner and flip assembly (bottom plots). The Baffle plot shows the temperature at different positions on the inner and outer baffles. Each dot represents the average temperature in one orbit. ---------- 8

Figure 3: SLSTR-A detector temperatures for each channel for the last month of operations. The vertical dashed lines indicate the start of each month. Each dot represents the average temperature in one orbit. The different colours indicate different detectors.---------- 9

Figure 4: SLSTR-B detector temperatures for each channel for the last month of operations. The vertical dashed lines indicate the start of each month. Each dot represents the average temperature in one orbit. The different colours indicate different detectors.---------- 10

Figure 5: SLSTR-A scanner and flip jitter for October 2023, showing mean and stddev from expected position per orbit (red and blue respectively) for the nadir view (left) and oblique view (right). The plots show the nadir scanner (top), oblique scanner (middle) and flip mirror (bottom).---------- 11

Figure 6: SLSTR-B scanner and flip jitter for October 2023, showing mean and stddev difference from expected position per orbit (red and blue respectively) for the nadir view (left) and oblique view (right). The plots show the nadir scanner (top), oblique scanner (middle) and flip mirror (bottom).---------- 12

Figure 7: SLSTR-A and SLSTR-B long term trends in average +YBB temperature, showing yearly variation. The vertical dashed lines indicate the 1st January in each year.---------- 13

Figure 8: SLSTR-A blackbody temperature and baseplate gradient trends during October 2023 measured by different sensors at various positions in the BB and Baseplate. Each dot represents the average temperature in one orbit. ---------- 14

Figure 9: SLSTR-B blackbody temperature and baseplate gradient trends during October 2023 measured by different sensors at various positions in the BB and Baseplate. Each dot represents the average temperature in one orbit. ---------- 15

Figure 10: VIS channel signal-to-noise of the measured VISCAL signal in each orbit for the last year of operations for SLSTR-A. Different colours indicate different detectors. The vertical dashed lines indicate the start of each month. ---------- 17

Figure 11. SWIR channel signal-to-noise of the measured VISCAL signal in each orbit for the last year of operations for SLSTR-A. Different colours indicate different detectors. The vertical dashed lines indicate the start of each month. ---------- 18

Figure 12: VIS channel signal-to-noise of the measured VISCAL signal in each orbit for the last year of operations for SLSTR-B. Different colours indicate different detectors. The vertical dashed lines indicate the start of each month. ---------- 20

Figure 13. SWIR channel signal-to-noise of the measured VISCAL signal in each orbit for the last year of operations for SLSTR-B. Different colours indicate different detectors. The vertical dashed lines indicate the start of each month. ---------- 21

Figure 14: SLSTR-A NEDT trend for the thermal channels in October 2023. Blue points were calculated from the cold blackbody signal and red points from the hot blackbody. The square symbols show results calculated from the nadir view and crosses show results from the oblique view. Results are plotted for all detectors and integrators, which is why there are several different levels within the same colour points (particularly for S8 and F2). ---------- 22

Figure 15: SLSTR-B NEDT trend for the thermal channels in October 2023. Blue points were calculated from the cold blackbody signal and red points from the hot blackbody. The square symbols show results calculated from the nadir view and crosses show results from the oblique view. Results are plotted for all detectors and integrators, which is why there are several different levels within the same colour points (particularly for S8 and F2). A blackbody cross over test was performed this month, which can be observed in the data near the 4-5th. ---------- 24

Figure 16: Variation of the radiometric gain derived from the VISCAL signals for SLSTR-A VIS channels for the last year of operations (nadir view). Different colours represent different detectors. The vertical dashed lines indicate the start of each month. ---------- 27

Figure 17: Variation of the radiometric gain derived from the VISCAL signals for SLSTR-A SWIR channels for the last year of operations (nadir view). Different colours represent different detectors. The vertical dashed lines indicate the start of each month. ---------- 28

Figure 18: Variation of the radiometric gain derived from the VISCAL signals for SLSTR-B VIS channels for the past year (nadir view). Different colours represent different detectors. The vertical dashed lines indicate the start of each month. ---------- 29

Figure 19: Variation of the radiometric gain derived from the VISCAL signals for SLSTR-B SWIR channels for the past year (nadir view). Different colours represent different detectors. The vertical dashed lines indicate the start of each month. ---------- 30

Figure 20: Daytime combined SLSTR-A and SLSTR-B Level-1 image for visible channels on 31st of October 2023. ---------- 31

Figure 21: Time-series of the elementary ratios (observed/simulated) signal from SLSTR-A for (top to bottom) bands S02 and S03 (Nadir & Oblique views) respectively over January 2023- mid-October 2023 from the six PICS Cal/Val sites. Dashed-green and orange lines indicate the 2% and 5% respectively. Error bars indicate the desert methodology uncertainty. ---------- 34

Figure 22: Time-series of the elementary ratios (observed/simulated) signal from SLSTR-B for (top to bottom) bands S02 and S03 (Nadir & Oblique views) respectively over January 2023- mid-October 2023 from the six PICS Cal/Val sites. Dashed-green and orange lines indicate the 2% and 5% respectively. Error bars indicate the desert methodology uncertainty. ---------- 36

Figure 23: The estimated gain values for SLSTR-A and SLSTR-B (top to bottom) Nadir & Oblique views respectively over the 6 PICS sites identified by CEOS over the period January 2023- mid-October 2023 as a function of wavelength. Dashed-green and orange lines indicate the 2% and 5% respectively. Error bars indicate the desert methodology uncertainty. ---------- 38

Figure 24: The estimated gain values for SLSTR-A and SLSTR-B (Nadir view) from Glint and Rayleigh methods over the period Jan 2022—mid-October 2023 and PICS method over the period Jan 2023—mid-October 2023 as a function of wavelength. We use the gain value of S02 from Desert-PICS method as reference gain for Glint method. Dashed-green and orange lines indicate the 2% and 5% respectively. Error bars indicate the method uncertainties. ---------- 39

Figure 25: Ratio of observed TOA reflectance to simulated one for (black) MERIS, (pale-green) S2A/MSI, (white) S2B/MSI, (blue) S3A/OLCI, (green) S3B/OLCI, (red) S3A/SLSTR-NADIR, and (cyan) S3B/SLSTR-NADIR averaged over the six PICS test sites as a function of wavelength.---------- 40

Figure 26: SLSTR-A daily offset results in km from the GeoCal Tool analysis for Nadir along- and across-track (top two plots) and Oblique along- and across-track (bottom two plots) for October 2023. The error bars show the standard deviation. ---------- 41

Figure 27: SLSTR-B daily offset results in km from the GeoCal Tool analysis for Nadir along- and across-track (top two plots) and Oblique along- and across-track (bottom two plots) for October 2023. The error bars show the standard deviation. ---------- 42

Figure 28: Validation of the SL_2_LST product in Q3 2023 for SLSTR-A (left) and SLSTR-B (right) at twelve Gold Standard in situ stations of the SURFRAD network plus two Gold Standard station from the ARM network. The matchups are split between daytime (red) and night-time (blue). ---------- 47

Figure 29: Intercomparison of the SL_2_LST product with respect to the operational LSA SAF SEVIRI LST product for December 2022 for SLSTR-A (left) and SLSTR-B (right). Daytime composites are in the top row and Night-time composites are in the bottom row. ---------- 49

Figure 30: Monthly composites at 0.05° of LST for December 2022 for SLSTR-A (left) and SLSTR-B (right). Daytime composites are in the top row and Night-time composites are in the bottom row.---------- 50

Figure 31: Formation process of the pairs of superclusters depending on AFP detected each satellite. Fire clusters and superclusters are identified by their colors. At the end of the process, pairs of SLSTR and MODIS superclusters share the same color. ---------- 53

Figure 32: Selected zones for the intercomparison over the July-September 2023 period ---------- 54

Figure 33: Fires detected by SLSTR and MODIS at nightime (left) and daytime (right). ---------- 54

Figure 34: For nighttime: (left) in red, the histogram of all FRP estimated from SLSTR; in blue and orange, a breakdown between commissions and double detections, respectively. (right) in red, the histogram of all FRP estimated from MODIS; in blue and orange, a breakdown between commissions and double detections, respectively. ---------- 55

Figure 35: Comparison between the FRP of cluster pairs detected by SLSTR and MODIS during nighttime ---------- 56

Figure 36: Comparison between the FRP of cluster pairs detected by SLSTR MWIR and SWIR bands during nighttime. ---------- 57

Figure 37: From left to right, for daytime: histograms of the FRP of fires detected by SLSTR and MODIS, histogram of the FRP of commissions, histogram of the FRP of omissions. ---------- 58

Figure 38: Comparison between the FRP of cluster pairs detected by SLSTR and MODIS during daytime. ---------- 58

Figure 39: Occurrences of commissions and omissions of active fire pixels per biome. On the left, nighttime; on the right, daytime. ---------- 59

List of Tables

Table 1: Average SLSTR-A reflectance factor, and signal-to-noise ratio of the measured VISCAL signal for the last 11 months, averaged over all detectors for the nadir view.---------- 16

Table 2: Average SLSTR-A reflectance factor, and signal-to-noise ratio of the measured VISCAL signal for the last 11 months, averaged over all detectors for the oblique view. ---------- 16

Table 3: Average SLSTR-B reflectance factor, and signal-to-noise ratio of the measured VISCAL signal for the last 11 months, averaged over all detectors for the nadir view.---------- 19

Table 4: Average SLSTR-B reflectance factor, and signal-to-noise ratio of the measured VISCAL signal for the last 11 months, averaged over all detectors for the oblique view. ---------- 19

Table 5: NEDT for SLSTR-A in the last 11 months averaged over all detectors for both Earth views towards the hot +YBB (top) and the cold -YBB (bottom). ---------- 23

Table 6: NEDT for SLSTR-B in the last 11 months averaged over all detectors for both Earth views towards the hot +YBB (top) and the cold -YBB (bottom). ---------- 25

Table 7. The recommended corrections that should be applied to SLSTR-A and SLSTR-B VIS, SWIR channels. ---------- 32

Table 8: Average absolute accuracy in K of the SL_2_LST product with respect to Gold Standard stations for Q3 2023.---------- 43

Table 9: Median differences in K from the intercomparison of the SL_2_LST product with respect to the operational LSA SAF SEVIRI LST product for December 2022---------- 48

Table 10: Summary of the intercomparison between nighttime SLSTR and MODIS active fires over the July—September 2023 period. Results from previous 3-months comparisons are included for information purposes. ---------- 55

Table 11: Summary of the intercomparison between daytime SLSTR and MODIS active fires over the July-September 2023 period. Results from previous 3-months comparisons are included for information purposes. ---------- 58

1 Executive Summary

This section provides a summary of the data quality for SLSTR-A and SLSTR-B over the month of operation.

Any relevant formal instrument data requirements are added under the subsequent section headers for reference.

Each month the data measured by SLSTR-A and SLSTR-B are checked for quality and it is determined whether they meet the requirements specified in Sentinel-3 Mission Requirements Document, using the methods in the Sentinel-3 Cal-Val Plan.

A summary of the status from each check performed is provided below. A traffic light system is used, where the categories are determined as follows

- Gray indicates no change over the reporting period
- Green indicates that aspect is performing optimally
- Amber indicates there are some issues noted that may affect data quality or availability this month, or a user correction that needs to be applied
- Red indicates a significant quality issue, or instrument anomaly for some of the month

Follow the link on each topic header for more detailed information contained in this document.

Topic	Instrument	Comments
Processing Baseline Version	S3A	
	S3B	
Event	S3A	Several events occurred this month without impact on data quality
	S3B	Several events occurred this month without impact on data quality, including a BB cross over test performed on 04-05/10
Instrument status	S3A	
	S3B	
Level-1 TIR Radiometric Validation	S3A	
	S3B	
Level-1 VIS SWIR Radiometric Validation	S3A	Vicarious validation indicates calibration offsets need to be applied to the VIS/SWIR channels New validation results using PICS method
	S3B	Vicarious validation indicates calibration offsets need to be applied to the VIS/SWIR channels New validation results using PICS method
Level-1 Geometric Validation	S3A	
	S3B	
Level-2 LST Validation	S3A	

Topic	Instrument	Comments
	S3B	
Level-2 FRP Validation	S3A	
	S3B	

2 Processing status

2.1 Processing baseline status

The Processing Baseline Version allows traceability of any changes to the software used to process the SLSTR products, and any updates to the auxiliary data files used to generate them.

The processing baseline identifier is now provided in the manifest file and in the global attributes of each file. The identifier comprises of seven characters (e.g. SL__L1_) which indicates the product type, and seven characters to indicate its version, xxx.yy.zz (e.g. 004.04.00). The version number, xxx indicates baseline collection, yy indicates change due to the IPF or ADF and zz indicates change in system components (e.g. L0, PUG) that do not impact data quality but are included to allow full traceability.

There has been no delivery or deployment concerning SLSTR during this period. The deployed processing baseline and IPF versions are consistent with the latest delivered versions.

IPF	IPF / Processing Baseline version	Date of deployment
S3A		
SL1	06.21 / SL__L1_.004.06.00	25/07/2023
SL2 LST	06.21 / SL__LST.004.08.02	25/07/2023
SL2 FRP (NTC)	01.08 / FRP_NTC.004.08.02	25/07/2023

IPF	IPF / Processing Baseline version	Date of deployment
S3B		
SL1	06.21 / SL__L1_.004.06.00	18/07/2023
SL2 LST	06.21 / SL__LST.004.08.02	18/07/2023
SL2 FRP (NTC)	01.08 / FRP_NTC.004.08.02	18/07/2023

No deployment has been done this month.
The Processing Baselines of S3A and S3B are aligned with the latest processing baseline version.

2.2 Processing anomalies

Only one specific issue has been identified this month on SLSTR, regarding FRP processing (OMPC-1539). Following the validation outcomes, some issues have been detected on the SWIR/MWIR clustering approach and the computation of the associated MWIR FRP value for each SWIR detected fires. A complete review of the code and the algorithm is on-going in collaboration between L2 Maintenance and ESLs.

A single issue has been raised this month regarding FRP SWIR/MWIR clustering approach. A complete review is on-going to understand and correct FRP_an.nc files.

3 Events and instrument anomalies

Any events that have occurred in this month that cause significant data gaps and impact on quality are reported here.

Some background to the typical events that might occur are provided below

- **RFI Radio Frequency Interference** occurs when another satellite causes the data downlink to the receiving station to be interrupted, and the data is lost.
- **Scheduled manoeuvres** may take place for Lunar views for calibration purposes, collision avoidance, or to maintain the nominal orbit. Will often result in the pointing flag being raised, and the geolocation accuracy is not nominal during this time.
- **Blackbody cross over tests** occur approximately once per year and the hot and cold blackbodies are swapped round for instrument testing.
- **De-icing** occurs when the instrument is heated to remove the build-up of ice.

3.1 SLSTR-A

SLSTR-A was switched on and operating nominally during October 2023, with Scan Unit Electronics (SUE) scanning and autonomous switching between day and night modes.

- 1st October, 16:22 – 16:24; 09th October, 19:22 – 19:34 and 19th October, 06:44 – 06:50 – Pointing Flags raised on oblique view only.
- 6th October, 21:45 – 21:54 – Data gaps due to RFI
- 11th October, 21:33 – 21:39 – Data gaps due to RFI
- 16th October, 08:11 – 08:26 – Pointing flag raised due to In-Plane manoeuvre.
- 31st October, 10:06 – 10:21 – Pointing flag raised due to In-Plane manoeuvre.

3.2 SLSTR-B

SLSTR-B was switched on and operating nominally during October 2023, with SUE scanning and autonomous switching between day and night modes.

However, starting on 04/10/2023 08:11 AM, a black body cross-over test has been executed and has impacted data for about 48 hours.

- 4th October, 08:07 – 5th October, 03:20 – Data gaps due to BB cross-over test
- 13th October, 08:45 – 09:02 – Pointing flag raised due to In-Plane manoeuvre.
- 14th October, 00:08 – 00:14 – data gaps due to RFI
- 29th October, 06:37 – 07:33 – data gaps and Pointing flag raised due to OLCI Moon Calibration

4 Instrument Status

The health of the instrument impacts the data quality. This section contains in depth analysis of several instrument parameters over the month of operation, and in some cases, the latest annual and mission tends for context.

SLSTR is a scanning radiometer, and uses two black bodies for thermal calibration, and a VISCAL unit for visible and shortwave IR calibration via the Sun. The key instrument properties that are monitored include:

- instrument temperature of the baffles
- instrument temperature of the Optical Mechanical Enclosure (optical bench, flip mirror and scan mirror, internal baffles)
- detector temperatures
- scanner and flip mirror performance

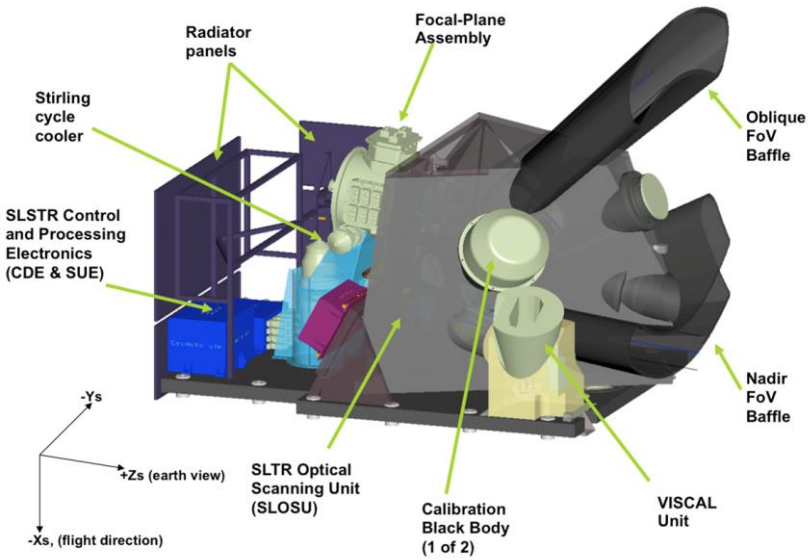

Sentinel 3 A

- The instrument was stable and compliant with requirements over much of the current month.

Sentinel 3 B

- The instrument was stable and compliant with requirements over the current month, with the exception of the period when a black body cross over test has been performed.

4.1 Instrument temperatures

As a thermal infrared instrument, thermal stability and uniformity of the optical mechanical enclosure (OME) is critical to the radiometric calibration. In this section we show the orbital average temperature of the OME and instrument baffles during the month. We expect to see a very small daily variation in temperature superimposed on a stable level over the month.

4.1.1 SLSTR-A

Figure 1 shows the orbital average temperature of the OME and instrument baffles for SLSTR-A during the month.

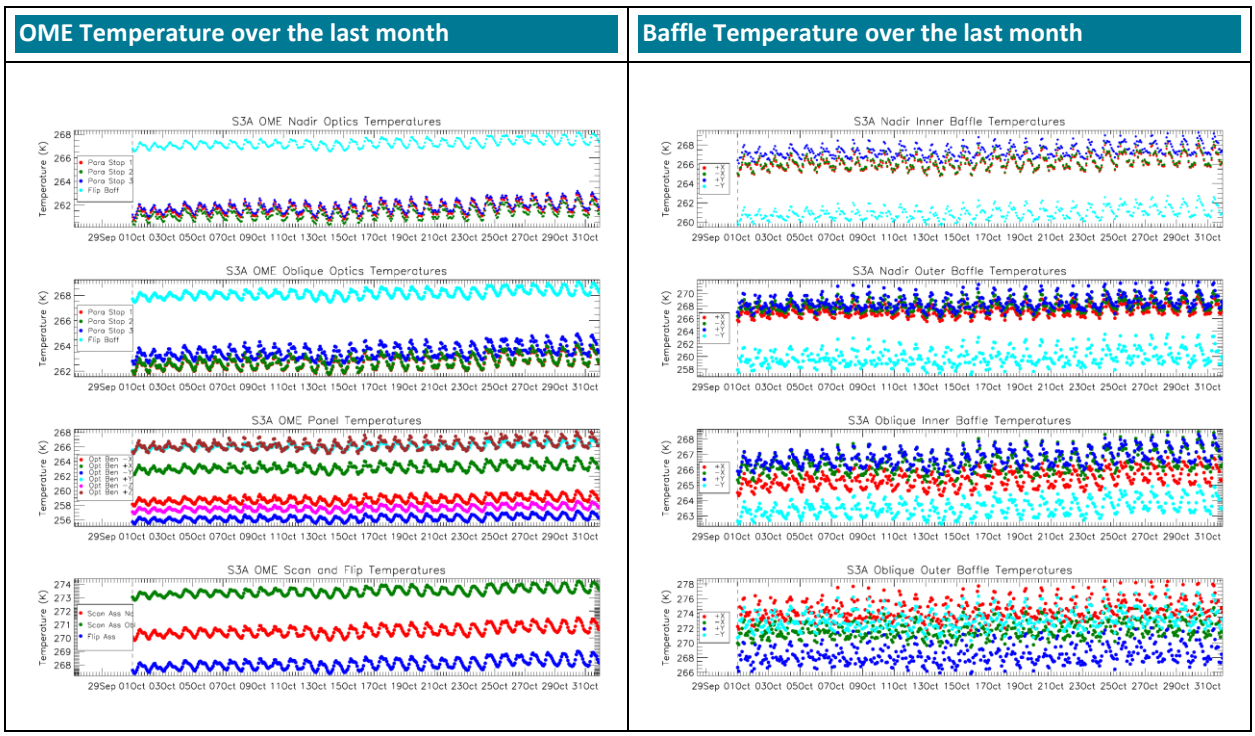

Figure 1: OME temperature trends for SLSTR-A (left) and Baffle temperature trends (right) during October 2023. The OME plot shows the three paraboloid stops and flip baffle (top two plots) and optical bench at different positions (third plots), and scanner and flip assembly (bottom plots). The Baffle plot shows the temperature at different positions on the inner and outer baffles. Each dot represents the average temperature in one orbit.

4.1.2 SLSTR-B

Figure 2 shows the orbital average temperature of the OME and instrument baffles for SLSTR-B during the month. The temperatures were stable (on top of a daily variation cycle).

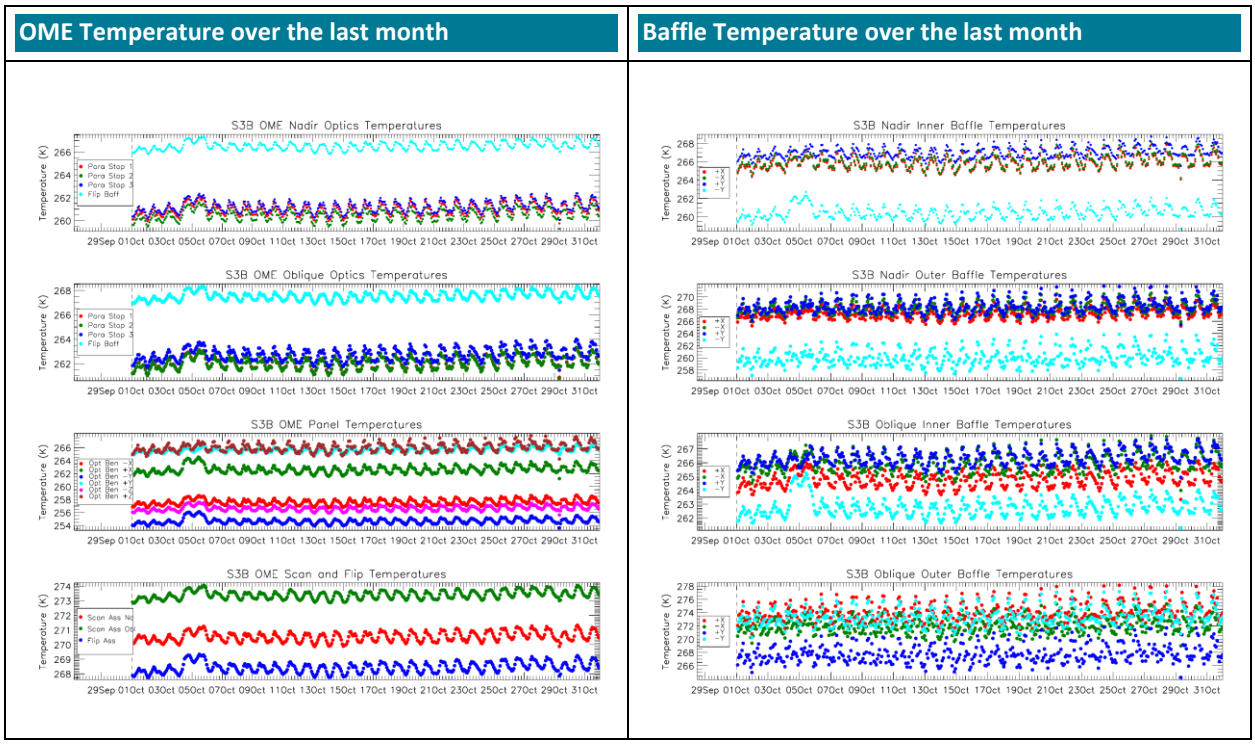

Figure 2: SLSTR-B OME temperature trends (left) and Baffle temperature trends (right) during October 2023. The OME plot shows the three paraboloid stops and flip baffle (top two plots) and optical bench at different positions (third plots), and scanner and flip assembly (bottom plots). The Baffle plot shows the temperature at different positions on the inner and outer baffles. Each dot represents the average temperature in one orbit.

4.2 Detector temperatures

The detector temperatures for both SLSTR-A and SLSTR-B were stable at their expected values over the month.

4.2.1 SLSTR-A

Figure 3 shows the annual trend in SLSTR-A detector temperatures for the past year. The temperatures from this month are consistent with the yearly trend.

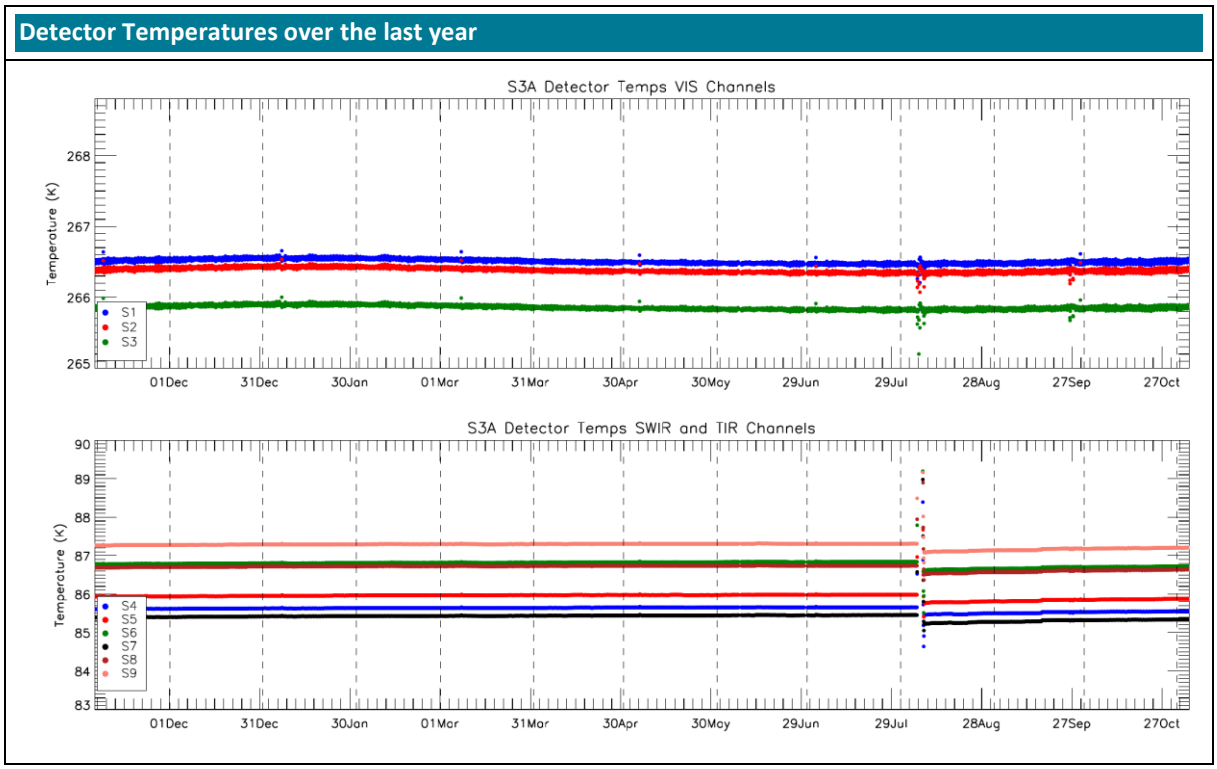

Figure 3: SLSTR-A detector temperatures for each channel for the last month of operations. The vertical dashed lines indicate the start of each month. Each dot represents the average temperature in one orbit. The different colours indicate different detectors.

4.2.2 SLSTR-B

Figure 4 shows the annual trend in SLSTR-B detector temperatures for the past year. The temperatures from this month are consistent with the yearly trend.

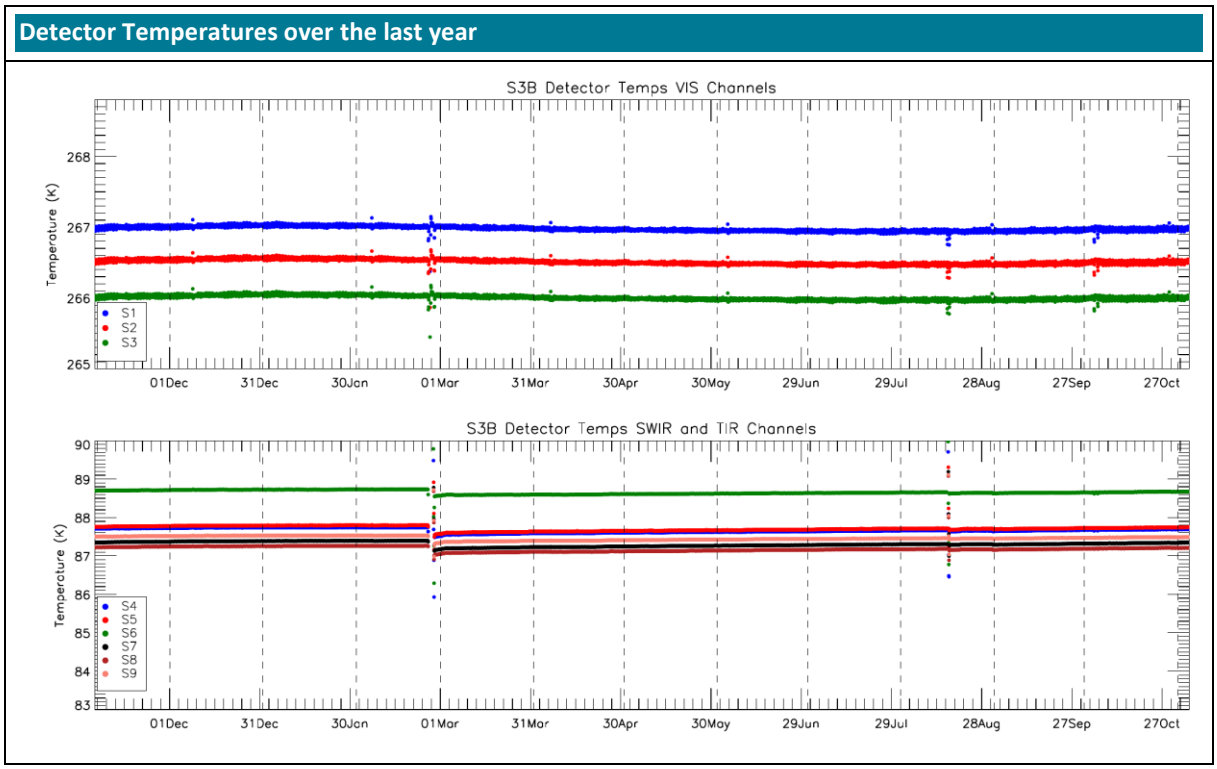

Figure 4: SLSTR-B detector temperatures for each channel for the last month of operations. The vertical dashed lines indicate the start of each month. Each dot represents the average temperature in one orbit. The different colours indicate different detectors.

4.3 Scanner performance

The actual position of the scan and flip mirrors is measured by the instrument, and in this section we show the statistics of the difference from the expected linear control law for each mirror in each view during October 2023. The performance has been consistent with previous operations and does not appear to be degrading. For reference, one arcsecond corresponds to roughly 4 m on the ground.

4.3.1 SLSTR-A

Figure 5 shows the statistics of the difference from the expected linear control law for each mirror in each view for SLSTR-A during the month.

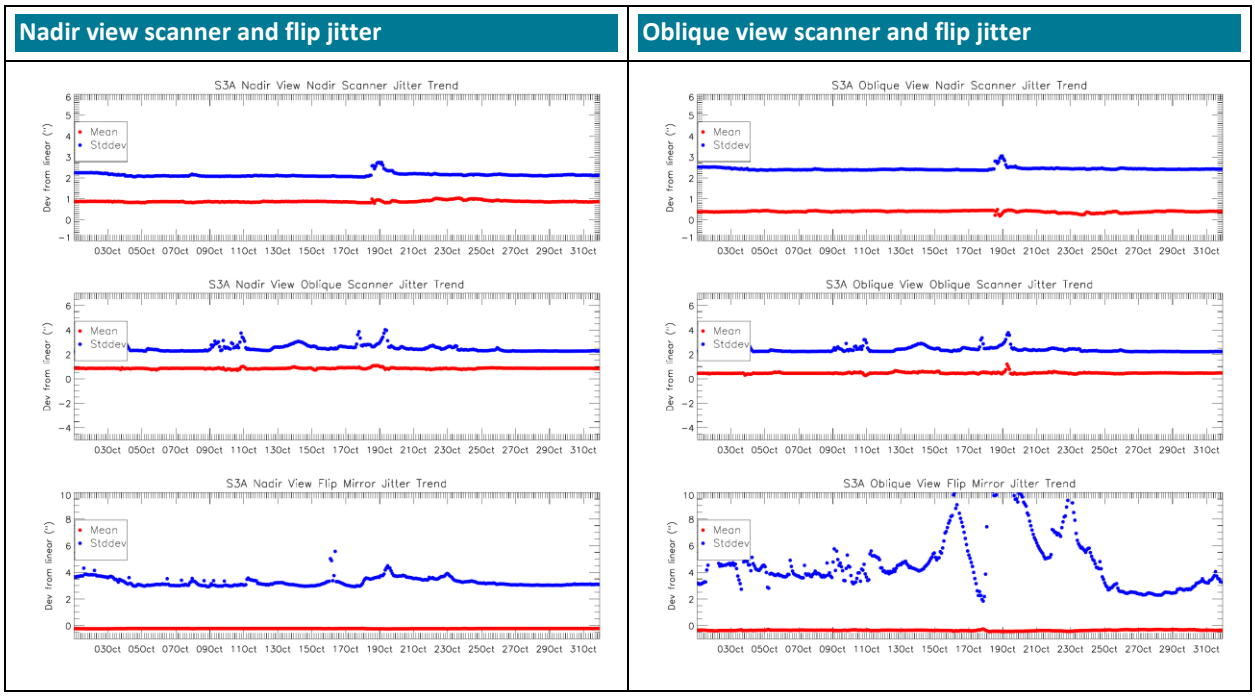

Figure 5: SLSTR-A scanner and flip jitter for October 2023, showing mean and stddev from expected position per orbit (red and blue respectively) for the nadir view (left) and oblique view (right). The plots show the nadir scanner (top), oblique scanner (middle) and flip mirror (bottom).

4.3.2 SLSTR-B

Figure 6 shows the statistics of the difference from the expected linear control law for each mirror in each view for SLSTR-B during the month.

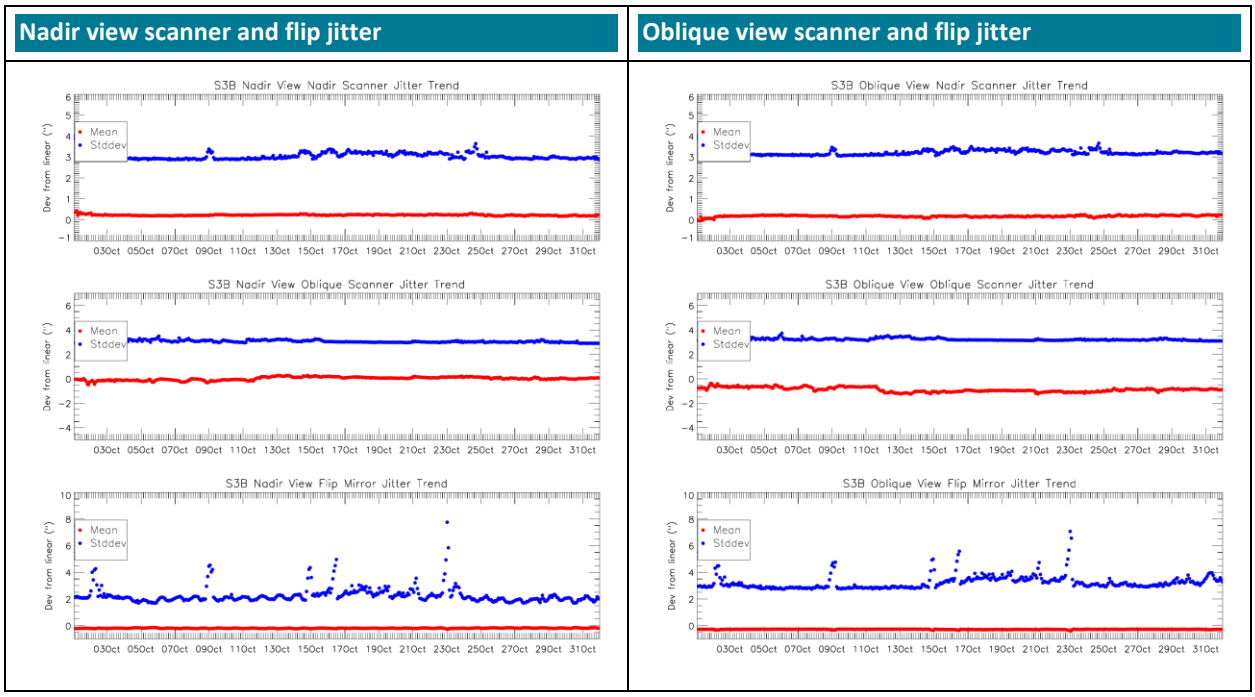

Figure 6: SLSTR-B scanner and flip jitter for October 2023, showing mean and stddev difference from expected position per orbit (red and blue respectively) for the nadir view (left) and oblique view (right). The plots show the nadir scanner (top), oblique scanner (middle) and flip mirror (bottom).

4.4 Black-Bodies

The monthly orbital average blackbody temperatures are shown in this section. The temperatures were stable on top of a daily variation cycle. There are also longer term trends which show a yearly variation, with temperatures rising as the Earth approaches perihelion at the beginning of January – this variation is shown in the monthly averages in Figure 7 and Table 5.

Latest mission trend of +Y hot BB temperature

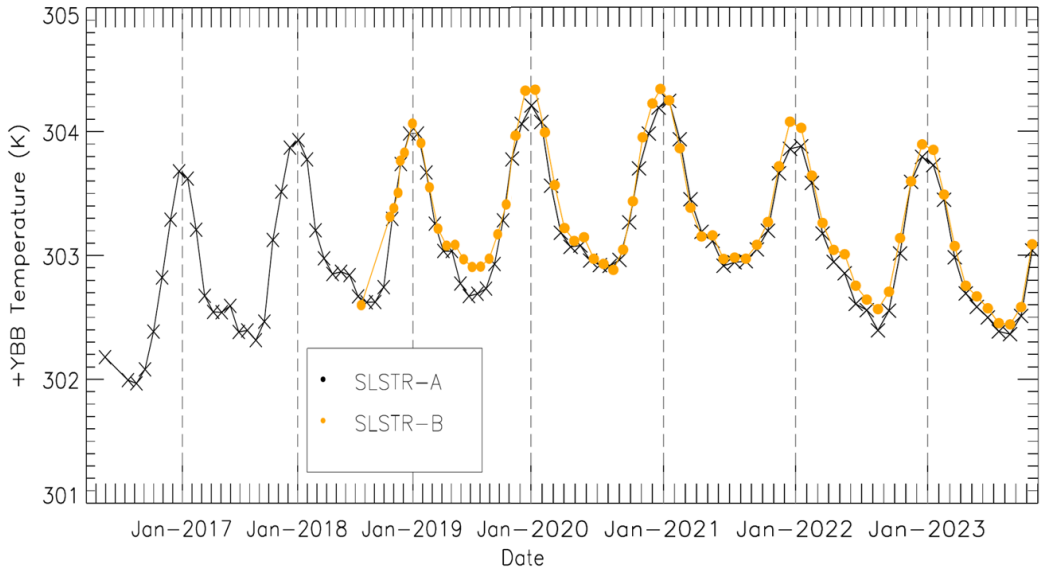

Figure 7: SLSTR-A and SLSTR-B long term trends in average +YBB temperature, showing yearly variation. The vertical dashed lines indicate the 1st January in each year.

4.4.1 SLSTR-A

The monthly orbital average blackbody temperatures for SLSTR-A are shown in Figure 8. The temperatures were stable on top of a daily variation cycle. Figure 8 also shows the gradients across the blackbody baseplate (i.e., each Platinum Resistance Thermometer (PRT) sensor reading relative to the mean). The gradients are stable and within their expected range of ±20mK.

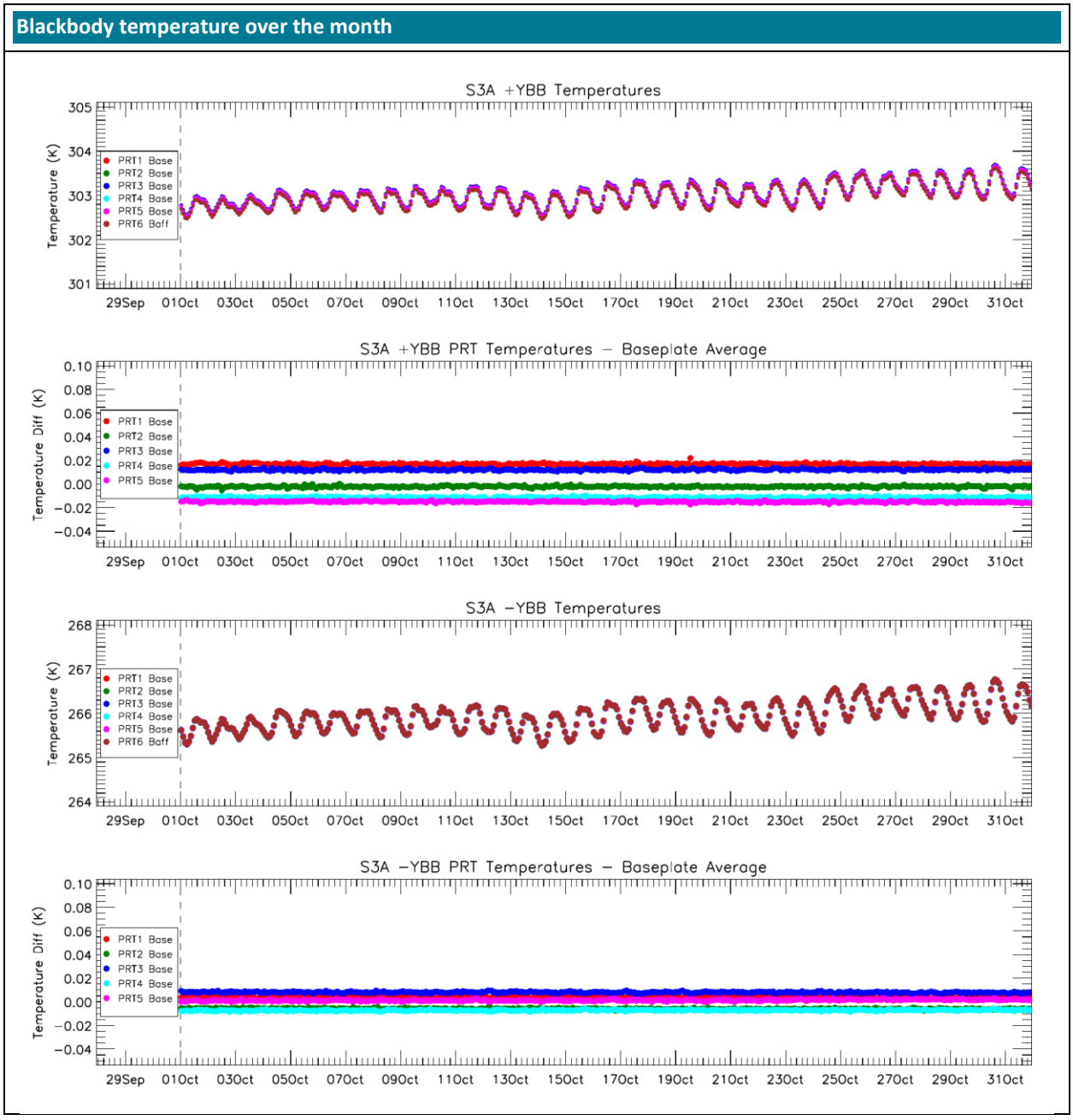

Figure 8: SLSTR-A blackbody temperature and baseplate gradient trends during October 2023 measured by different sensors at various positions in the BB and Baseplate. Each dot represents the average temperature in one orbit.

4.4.2 SLSTR-B

The monthly orbital average blackbody temperatures for SLSTR-B are shown in Figure 9. The temperatures were stable on top of a daily variation cycle, with the exception of the period of the Blackbody cross over test (4-5 th October). Figure 9 also shows the gradients across the blackbody baseplate (i.e., each Platinum Resistance Thermometer (PRT) sensor reading relative to the mean). The gradients are stable and within their expected range of ±20mK, except for the +Y blackbody for SLSTR-B which has a higher gradient. This higher gradient is expected and consistent with measurements made before launch.

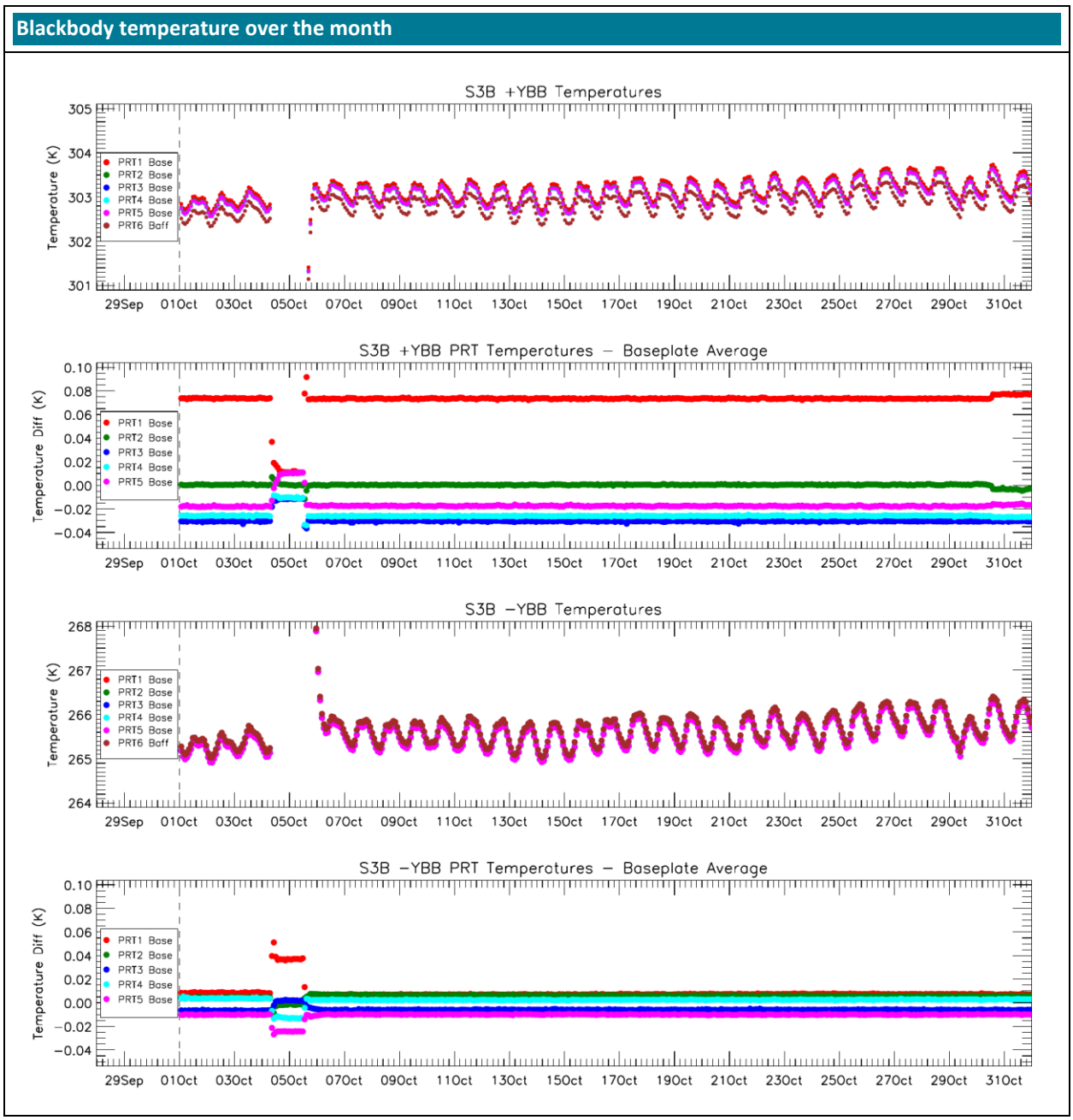

Figure 9: SLSTR-B blackbody temperature and baseplate gradient trends during October 2023 measured by different sensors at various positions in the BB and Baseplate. Each dot represents the average temperature in one orbit.

4.5 Detector noise levels

4.5.1 SLSTR-A VIS and SWIR channel signal-to-noise

The VIS and SWIR channel noise for SLSTR-A during October 2023 was stable and consistent with previous operations - the signal-to-noise ratio of the measured VISCAL signal over the past year is plotted in Figure 10 and Figure 11. Table 1 and Table 2 give the average monthly signal-to-noise (excluding the instrument decontaminations). These values average over the significant detector-detector dispersion for the SWIR channels that is shown in Figure 11. Note that these averages are now calculated for each calendar month, whereas in data quality reports before January 2022 they were aligned to the satellite 27 day repeat cycles.

Table 1: Average SLSTR-A reflectance factor, and signal-to-noise ratio of the measured VISCAL signal for the last 11 months, averaged over all detectors for the nadir view.

	Average Reflectance Factor	Nadir Signal-to-noise ratio										
		Dec 2022	Jan 2023	Feb 2023	Mar 2023	Apr 2023	May 2023	Jun 2023	Jul 2023	Aug 2023	Sep 2023	Oct 2023
S1	0.187	239	239	239	242	244	239	234	235	238	236	243
S2	0.194	246	246	243	241	243	243	242	241	242	241	243
S3	0.190	228	231	229	225	223	218	213	216	222	221	222
S4	0.191	173	174	172	171	170	166	164	164	168	171	173
S5	0.193	286	291	289	284	283	280	280	279	280	283	285
S6	0.175	186	187	185	183	181	180	178	178	181	183	184

Table 2: Average SLSTR-A reflectance factor, and signal-to-noise ratio of the measured VISCAL signal for the last 11 months, averaged over all detectors for the oblique view.

	Average Reflectance Factor	Oblique Signal-to-noise ratio										
		Dec 2022	Jan 2023	Feb 2023	Mar 2023	Apr 2023	May 2023	Jun 2023	Jul 2023	Aug 2023	Sep 2023	Oct 2023
S1	0.166	262	259	259	262	261	252	242	246	250	249	256
S2	0.170	271	268	262	260	258	255	250	256	257	256	259
S3	0.168	236	238	235	232	226	219	213	217	222	222	222
S4	0.166	140	139	138	138	138	137	134	136	138	139	139
S5	0.166	215	211	209	214	214	214	208	213	213	215	215
S6	0.155	133	131	129	131	131	131	130	129	132	134	134

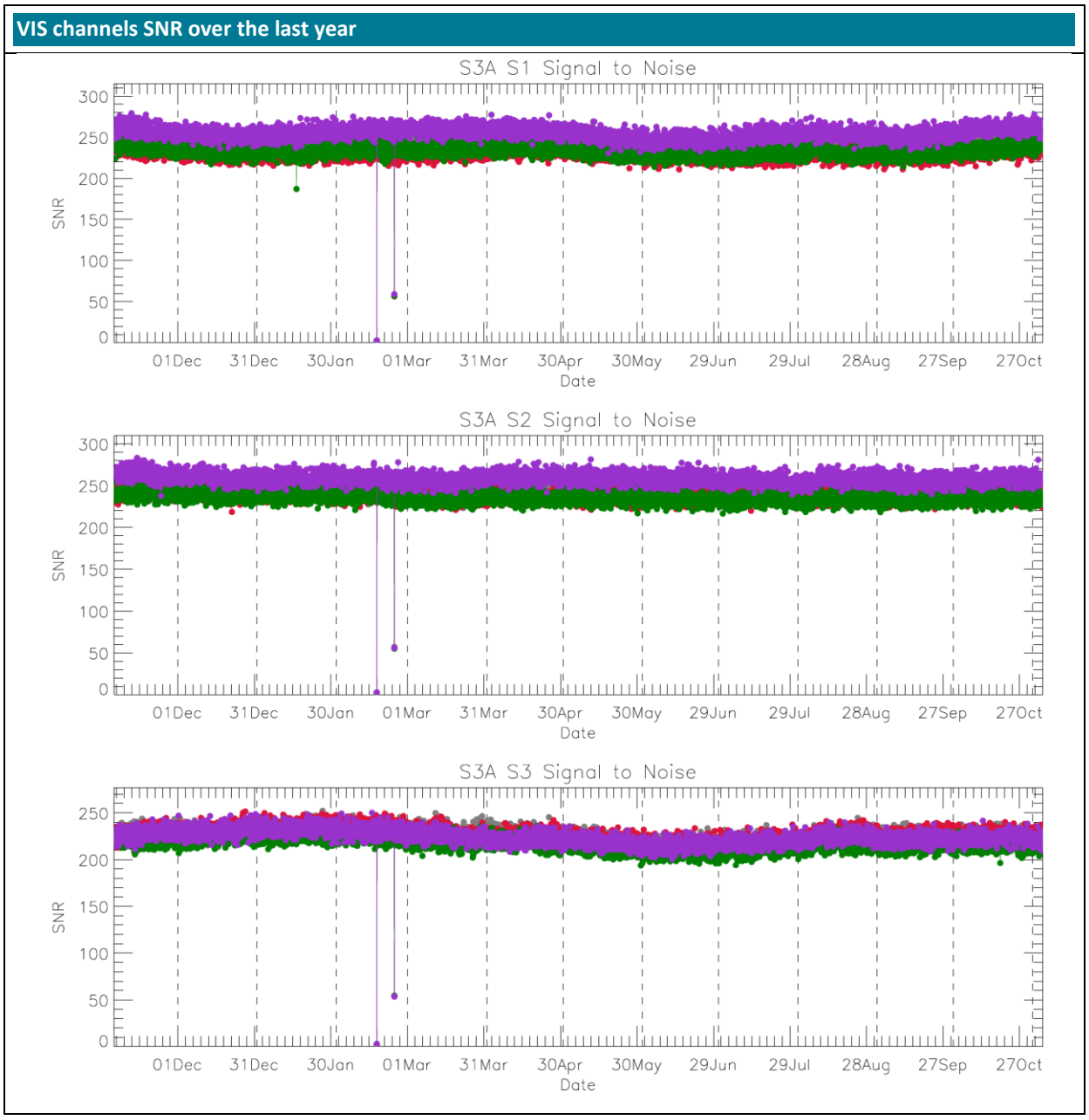

Figure 10: VIS channel signal-to-noise of the measured VISCAL signal in each orbit for the last year of operations for SLSTR-A. Different colours indicate different detectors. The vertical dashed lines indicate the start of each month.

SWIR SNR over the last year

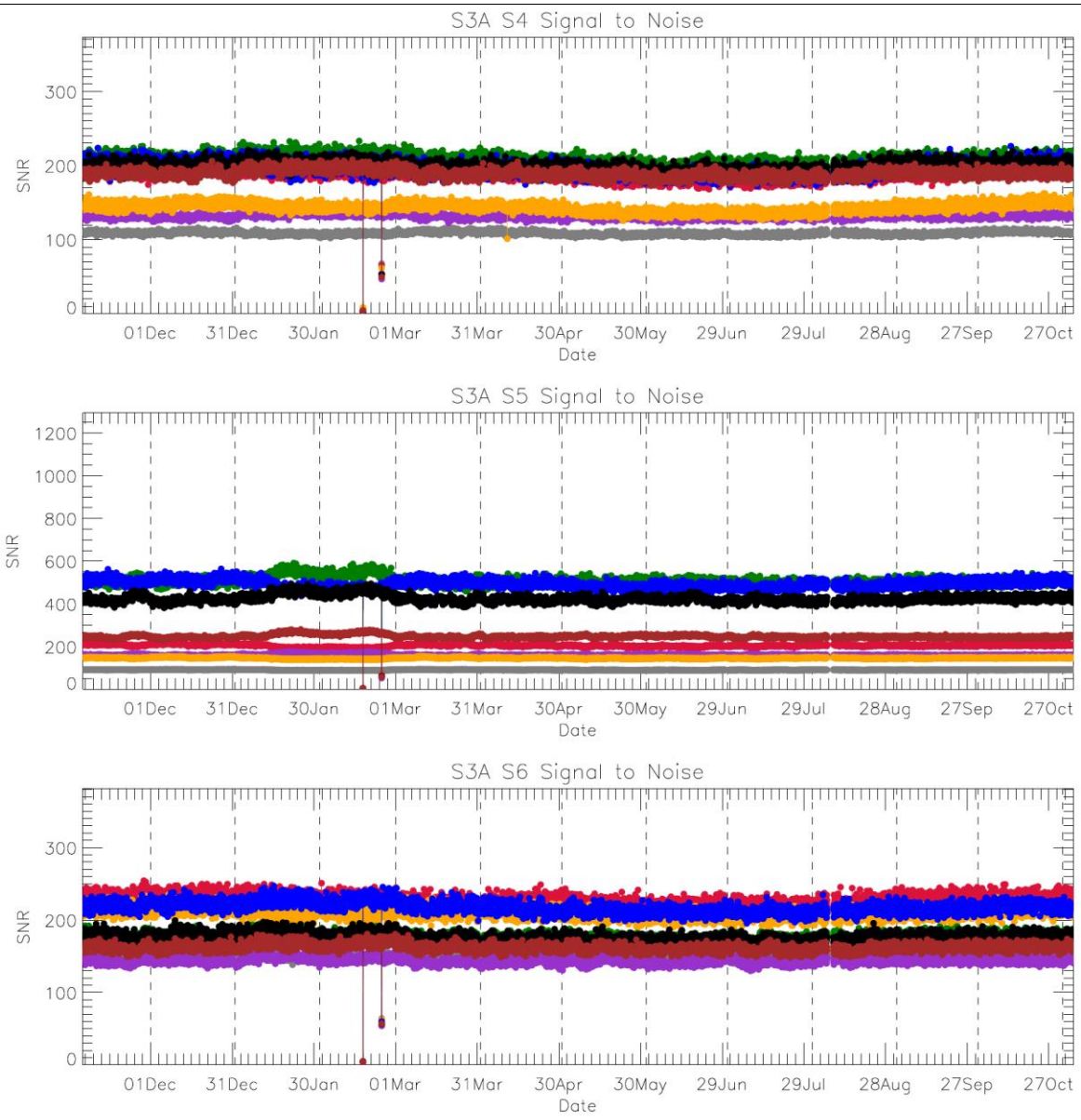

Figure 11. SWIR channel signal-to-noise of the measured VISCAL signal in each orbit for the last year of operations for SLSTR-A. Different colours indicate different detectors. The vertical dashed lines indicate the start of each month.

4.5.2 SLSTR-B VIS and SWIR channel signal-to-noise

The monthly average VIS and SWIR channel signal-to-noise ratios for SLSTR-B are shown in Table 3 and Table 4. These values average over a significant detector-detector dispersion for the SWIR channels.

Table 3: Average SLSTR-B reflectance factor, and signal-to-noise ratio of the measured VISCAL signal for the last 11 months, averaged over all detectors for the nadir view.

	Average Reflectance Factor	Nadir Signal-to-noise ratio										
		Dec 2022	Jan 2023	Feb 2023	Mar 2023	Apr 2023	May 2023	Jun 2023	Jul 2023	Aug 2023	Sep 2023	Oct 2023
S1	0.177	232	238	238	223	227	228	221	219	226	232	231
S2	0.192	223	221	221	218	215	214	216	214	215	217	221
S3	0.194	221	223	226	222	217	213	214	216	219	219	219
S4	0.186	131	131	130	129	129	128	126	126	126	127	127
S5	0.184	243	242	243	243	240	239	238	237	238	238	239
S6	0.162	163	165	165	162	161	159	159	157	159	158	158

Table 4: Average SLSTR-B reflectance factor, and signal-to-noise ratio of the measured VISCAL signal for the last 11 months, averaged over all detectors for the oblique view.

	Average Reflectance Factor	Oblique Signal-to-noise ratio										
		Dec 2022	Jan 2023	Feb 2023	Mar 2023	Apr 2023	May 2023	Jun 2023	Jul 2023	Aug 2023	Sep 2023	Oct 2023
S1	0.157	224	228	222	217	219	217	208	208	216	220	217
S2	0.168	257	256	255	251	245	245	245	241	242	246	255
S3	0.172	250	253	253	248	237	232	234	238	239	238	238
S4	0.168	133	132	131	131	130	127	124	126	126	128	128
S5	0.172	252	251	251	251	251	249	248	248	247	249	249
S6	0.152	189	188	186	188	187	182	180	180	182	184	185

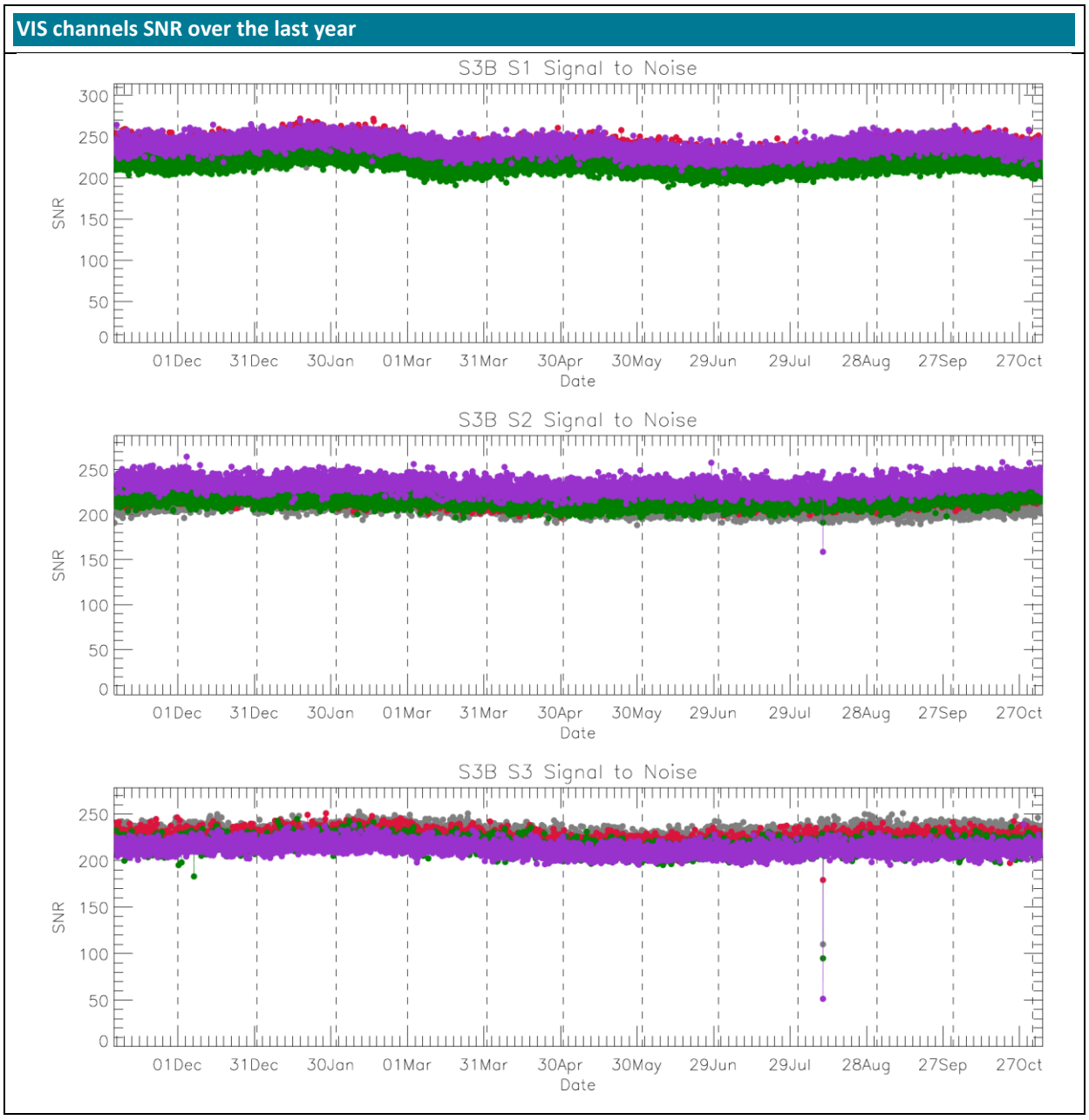

Figure 12: VIS channel signal-to-noise of the measured VISCAL signal in each orbit for the last year of operations for SLSTR-B. Different colours indicate different detectors. The vertical dashed lines indicate the start of each month.

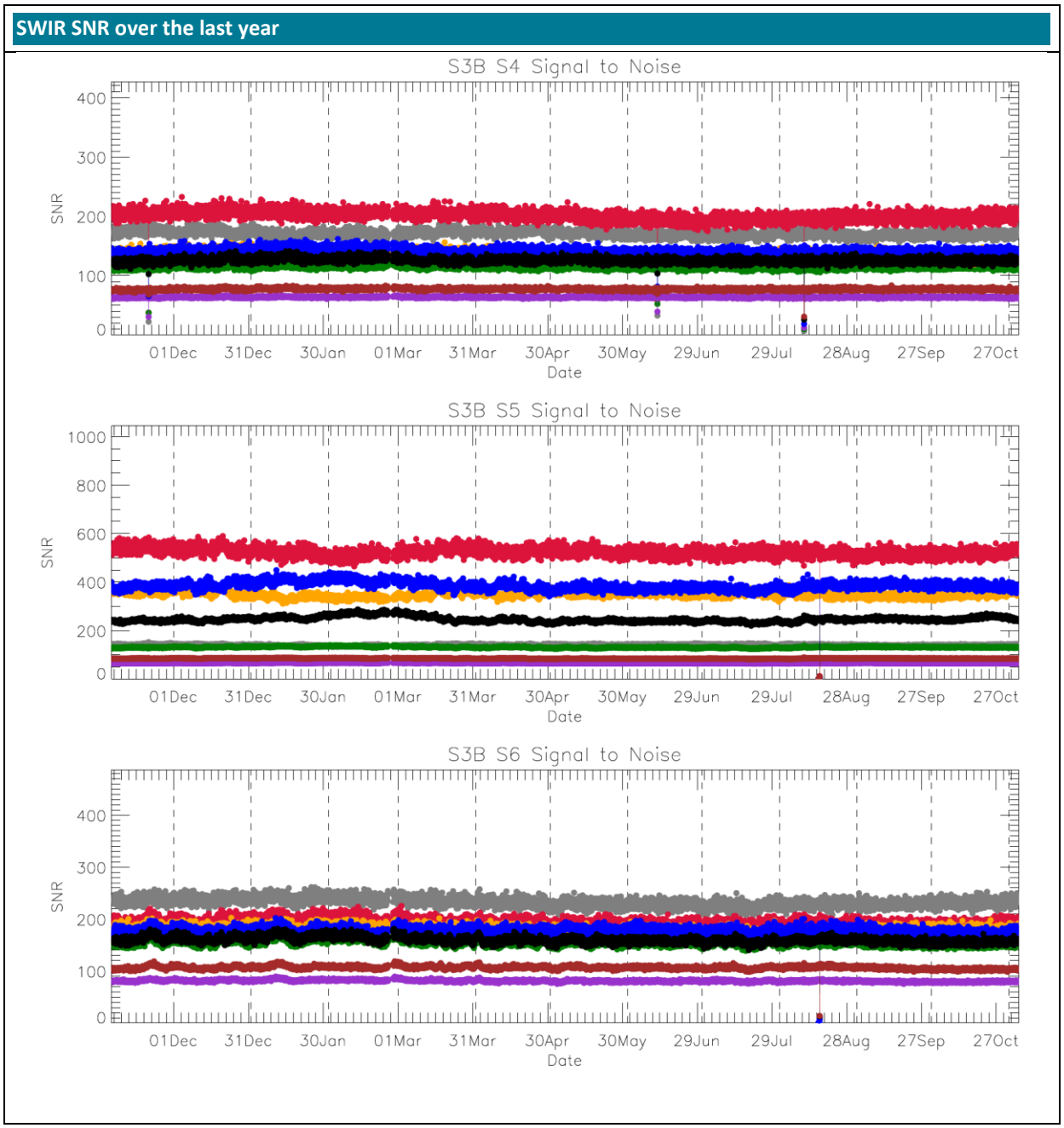

Figure 13. SWIR channel signal-to-noise of the measured VISCAL signal in each orbit for the last year of operations for SLSTR-B. Different colours indicate different detectors. The vertical dashed lines indicate the start of each month.

4.5.3 SLSTR-A TIR channel NEDT

The thermal channel NEDT values for SLSTR-A in October 2023 are consistent with previous operations and within the requirements. NEDT trends calculated from the hot and cold blackbody signals are shown in Figure 14. Monthly NEDT values, averaged over all detectors and both Earth views, are shown in Table 5.

TIR NEDT over the month

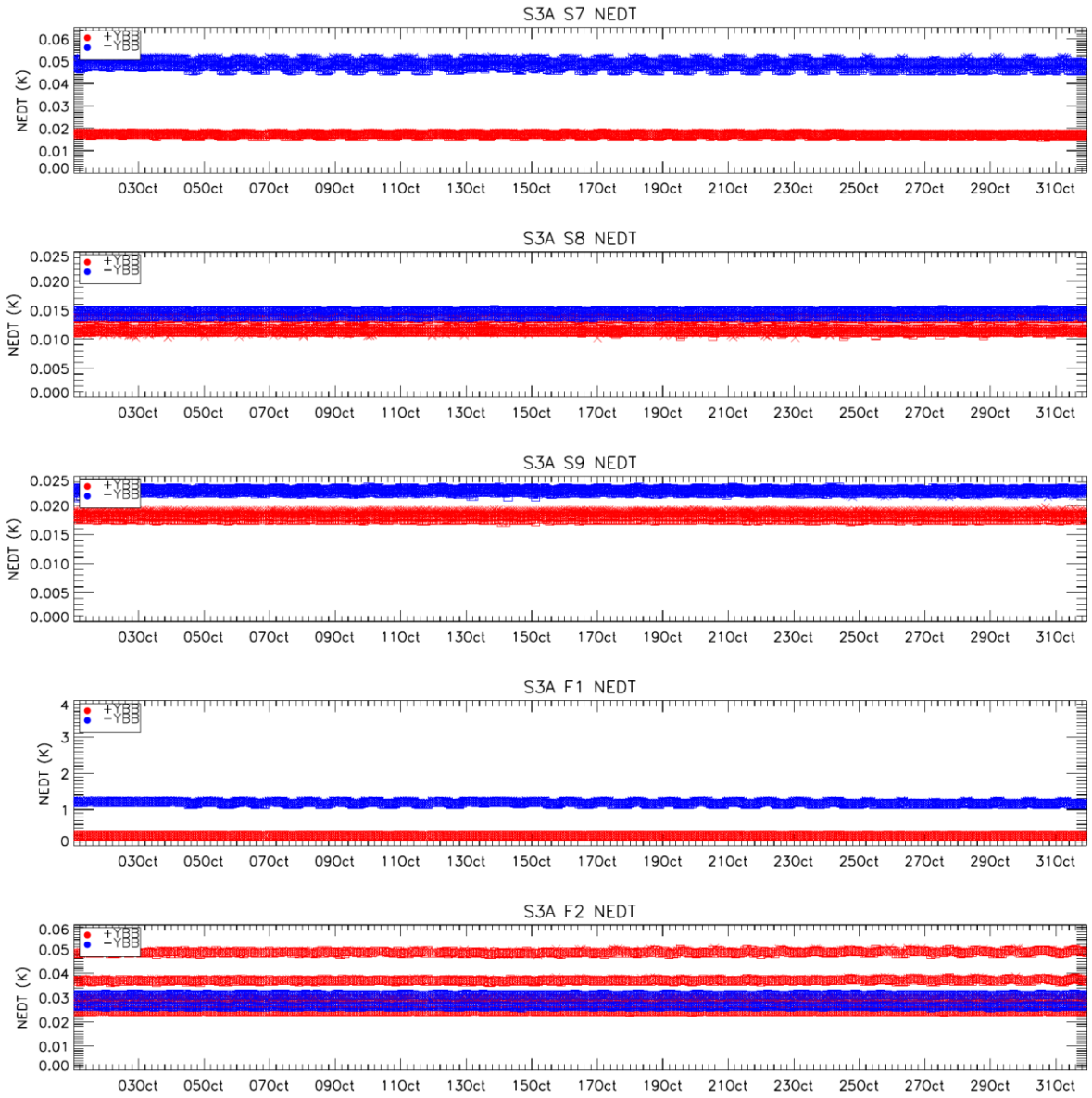

Figure 14: SLSTR-A NEDT trend for the thermal channels in October 2023. Blue points were calculated from the cold blackbody signal and red points from the hot blackbody. The square symbols show results calculated from the nadir view and crosses show results from the oblique view. Results are plotted for all detectors and integrators, which is why there are several different levels within the same colour points (particularly for S8 and F2).

Table 5: NEDT for SLSTR-A in the last 11 months averaged over all detectors for both Earth views towards the hot +YBB (top) and the cold -YBB (bottom).

SLSTR-A		Dec 2022	Jan 2023	Feb 2023	Mar 2023	Apr 2023	May 2023	June 2023	July 2023	Aug 2023	Sep 2023	Oct 2023
+YBB temp (K)		303.793	303.727	303.447	302.983	302.692	302.584	302.498	302.385	302.363	302.514	303.038
NEDT (mK)	S7	17.1	17.2	17.2	17.4	17.6	17.6	17.6	17.6	17.5	18.1	17.3
	S8	12.0	12.0	12.0	12.0	12.1	12.1	12.1	12.1	11.9	12.0	11.9
	S9	18.4	18.5	18.5	18.5	18.6	18.6	18.6	18.7	18.3	18.4	18.3
	F1	278	279	279	284	288	290	290	290	284	302	281
	F2	35.4	35.3	35.3	34.9	34.8	34.7	34.6	34.6	34.5	34.5	34.9

SLSTR-A		Dec 2022	Jan 2023	Feb 2023	Mar 2023	Apr 2023	May 2023	June 2023	July 2023	Aug 2023	Sep 2023	Oct 2023
-YBB temp (K)		266.812	266.695	266.319	265.801	265.594	265.630	265.589	265.224	265.201	265.299	265.941
NEDT (mK)	S7	47.6	48.0	48.5	49.4	50.1	50.4	50.2	49.8	49.8	48.3	48.7
	S8	14.6	14.6	14.6	14.7	14.7	14.7	14.7	14.7	14.6	14.5	14.6
	S9	22.6	22.7	22.7	22.8	22.9	23.0	23	23.1	22.6	22.4	22.5
	F1	1155	1169	1186	1218	1236	1245	1247	1243	1219	1187	1195
	F2	28.8	28.9	28.9	28.9	29.0	29.1	29.0	29.0	28.7	29.0	28.8

4.5.4 SLSTR-B TIR channel NEDT

The thermal channel NEDT values for SLSTR-B in October 2023, calculated from the hot and cold blackbody signals are shown in Figure 15 with monthly averages in Table 6. The thermal channel NEDT values for SLSTR-B in October 2023 are consistent with previous operations and within the requirements, except around 4-5 th of October where the impact of the Blackbody cross over test can be observed. Note that these averages are now calculated for each calendar month, whereas in data quality reports before January 2022 they were aligned to the satellite 27-day repeat cycles.

TIR NEDT over the month

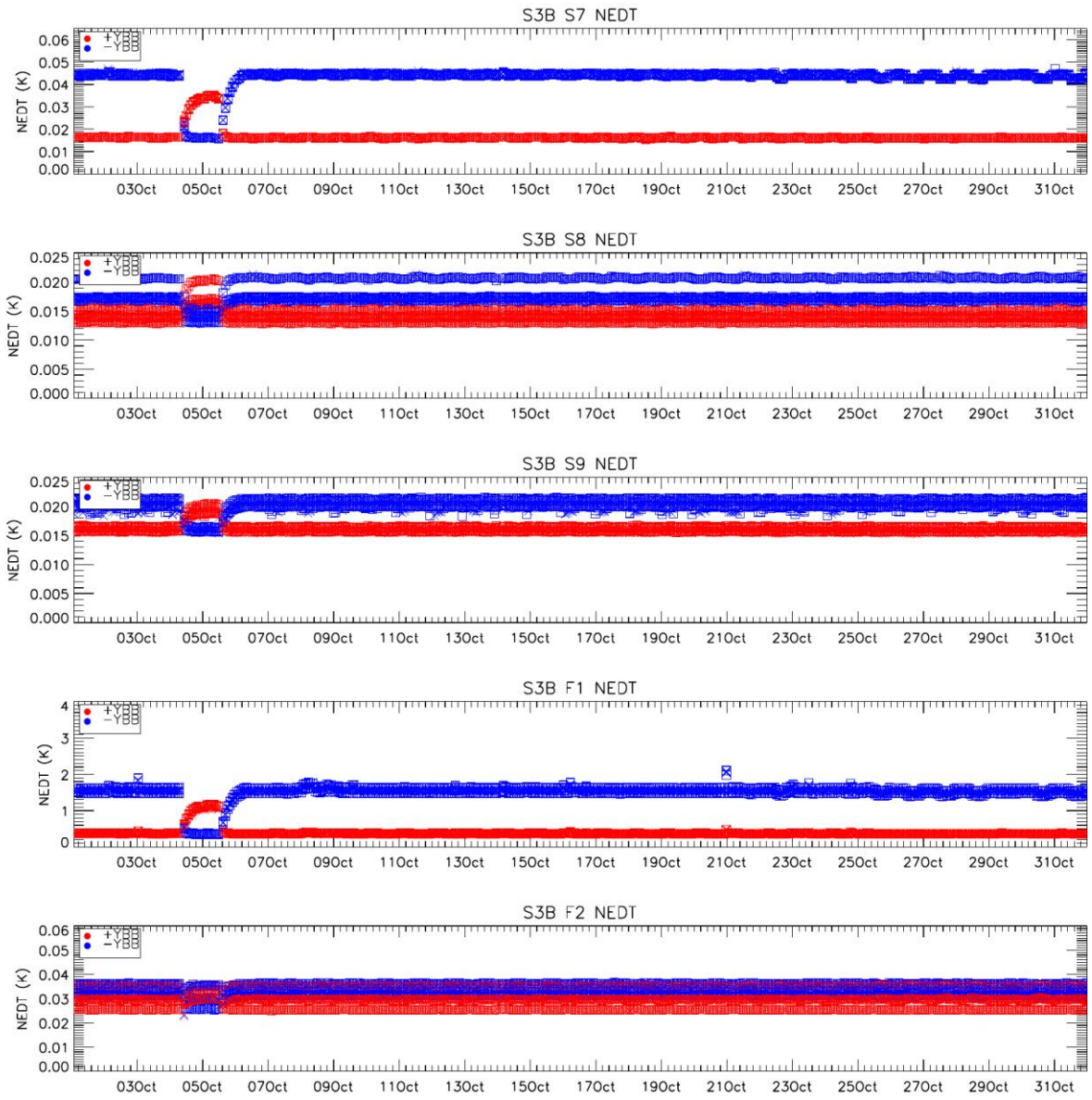

Figure 15: SLSTR-B NEDT trend for the thermal channels in October 2023. Blue points were calculated from the cold blackbody signal and red points from the hot blackbody. The square symbols show results calculated from the nadir view and crosses show results from the oblique view. Results are plotted for all detectors and integrators, which is why there are several different levels within the same colour points (particularly for S8 and F2). A blackbody cross over test was performed this month, which can be observed in the data near the 4-5th.

Table 6: NEDT for SLSTR-B in the last 11 months averaged over all detectors for both Earth views towards the hot +YBB (top) and the cold -YBB (bottom).

SLSTR-B		Dec 2022	Jan 2023	Feb 2023	Mar 2023	Apr 2023	May 2023	Jun 2023	Jul 2023	Aug 2023	Sep 2023	Oct 2023
+YBB temp (K)		303.894	303.850	303.489	303.074	302.754	302.668	302.572	302.452	302.442	302.582	303.582
NEDT (mK)	S7	16.1	16.0	16.1	16.2	16.5	16.5	16.5	16.5	16.5	16.5	16.8
	S8	14.3	13.9	14.0	14.0	14.0	14.0	14.0	14.1	14.1	14.0	14.1
	S9	16.5	15.9	16.0	15.8	15.8	15.9	15.9	16.0	16.0	16.0	16.1
	F1	345	349	369	367	368	367	369	374	378	380	393
	F2	30.6	30.5	30.4	30.2	30.3	30.3	30.2	30.1	30.1	30.1	30.2

SLSTR-B		Dec 2022	Jan 2023	Feb 2023	Mar 2023	Apr 2023	May 2023	Jun 2023	Jul 2023	Aug 2023	Sep 2023	Oct 2023
-YBB temp (K)		266.554	266.431	265.924	265.360	265.131	265.196	265.146	264.944	264.837	264.943	265.568
NEDT (mK)	S7	42.9	42.8	43.7	44.6	44.5	44.3	44.8	45.5	45.9	45.3	42.3
	S8	17.9	18.0	18.0	17.8	17.8	17.9	17.9	18.0	18.0	18.0	17.8
	S9	20.4	20.4	20.5	20.2	20.3	20.3	20.4	20.4	20.5	20.5	20.3
	F1	1427	1430	1564	1550	1525	1502	1529	1571	1592	1595	1503
	F2	33.1	33.2	33.3	33.1	33.1	33.2	33.3	33.4	33.4	33.3	33.1

4.6 Calibration factors

4.6.1 VIS and SWIR radiometric response

The radiometric gain derived from the VISCAL signals over the past year are shown in this section. It should be noted that the data from the VISCAL unit and blackbodies calibrates the signal and counteracts the degradation of the optics and other variations in signal observed in the plots.

There are several features that appear in this parameter that can be explained as:

- The visible channels show oscillations in their radiometric response due to the build-up of ice on the optical path within the focal plane assembly (FPA). Similar oscillations were observed for the corresponding channels on ATSR-2 and AATSR. As described in Section 4.2, periodic decontamination of the infrared FPA is necessary to remove the water ice contamination.
- The radiometric responses of the SWIR channels appear to be more stable and not affected by the build-up of water ice contamination, although there is a seasonal cycle of the response that could be caused by variations in the solar zenith angle on the diffuser or partial vignetting of the Sun's disc by the VISCAL baffle.
- Note that the period of the oscillations depends on the rate of build up of the ice layer, which is faster for SLSTR-B because it has had less time to decontaminate.

4.6.2 SLSTR-A

Figure 16 and Figure 17 show the variation of the radiometric gain derived from the VISCAL signals for SLSTR-A over the past year. The data from the last month appears normal and follows the expected trend. The following features in this annual trend plot should be noted:

- August 2023: an anomaly occurred on the instrument on 6st August, which was recovered with a power cycle and decontamination/cooldown. This causes a discontinuity in the gain due to the reduction in water ice after the decontamination.

VIS VISCAL signal variation over the past year

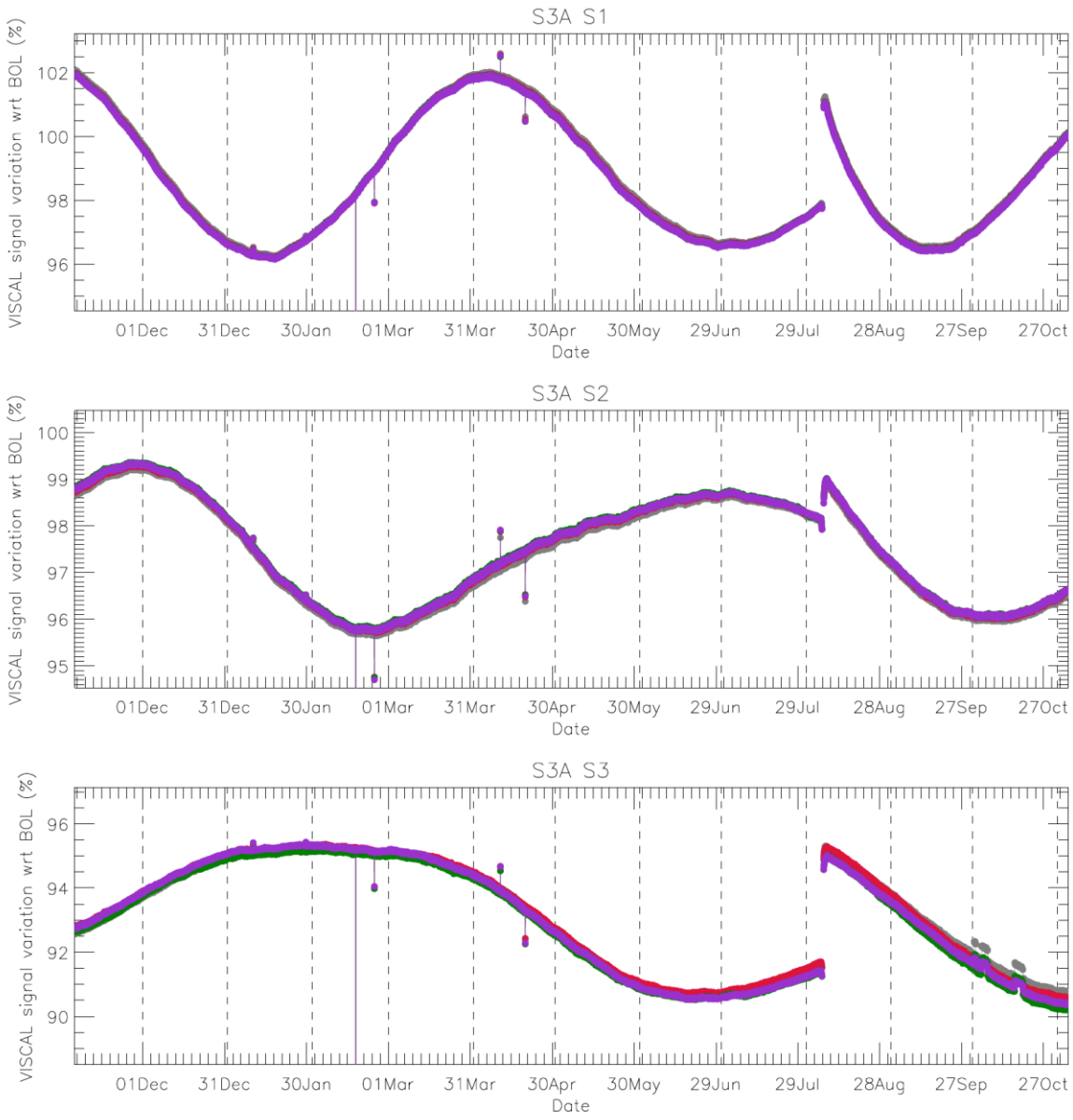

Figure 16: Variation of the radiometric gain derived from the VISCAL signals for SLSTR-A VIS channels for the last year of operations (nadir view). Different colours represent different detectors. The vertical dashed lines indicate the start of each month.

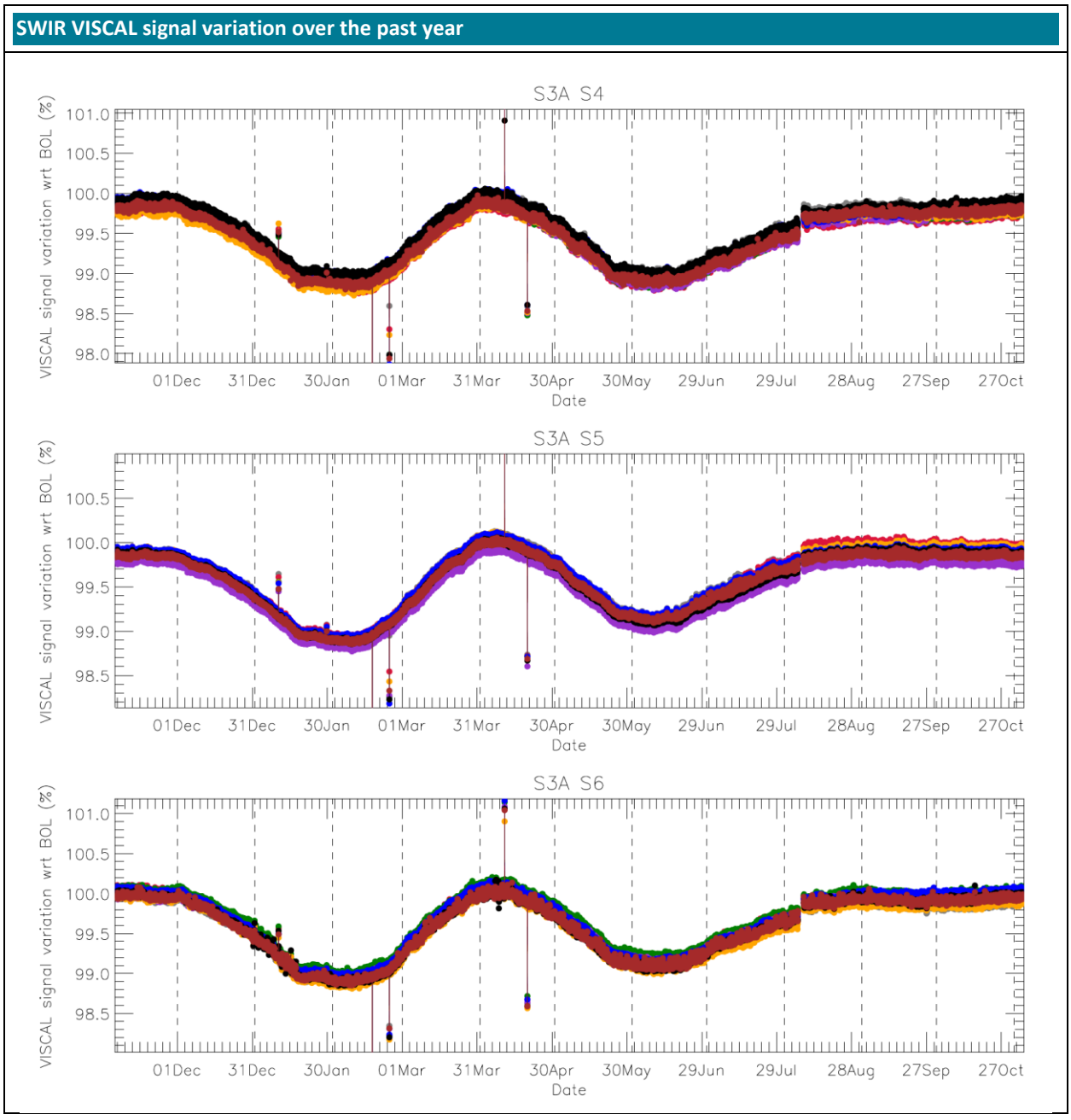

Figure 17: Variation of the radiometric gain derived from the VISCAL signals for SLSTR-A SWIR channels for the last year of operations (nadir view). Different colours represent different detectors. The vertical dashed lines indicate the start of each month.

4.6.3 SLSTR-B

Figure 18 and Figure 19 show the variation of the radiometric gain derived from the VISCAL signals for SLSTR-B over the past year. The data from the last month appears normal and follows the expected trend. There are several features in this annual trend plot to note.

- There is noisy behaviour and numerous drops in signal in the radiometric gain, especially in channels S1 and S2. This gives 2-3% errors in the radiometric calibration of these channels. A

number of candidate root causes have been identified, with the most likely due to motional chopping of the VIS detectors by an internal aperture in the VIS optical bench. Because the effect appears to be random it is most likely affecting all the data for S1 and S2.

VIS VISCAL signal variation over the past year

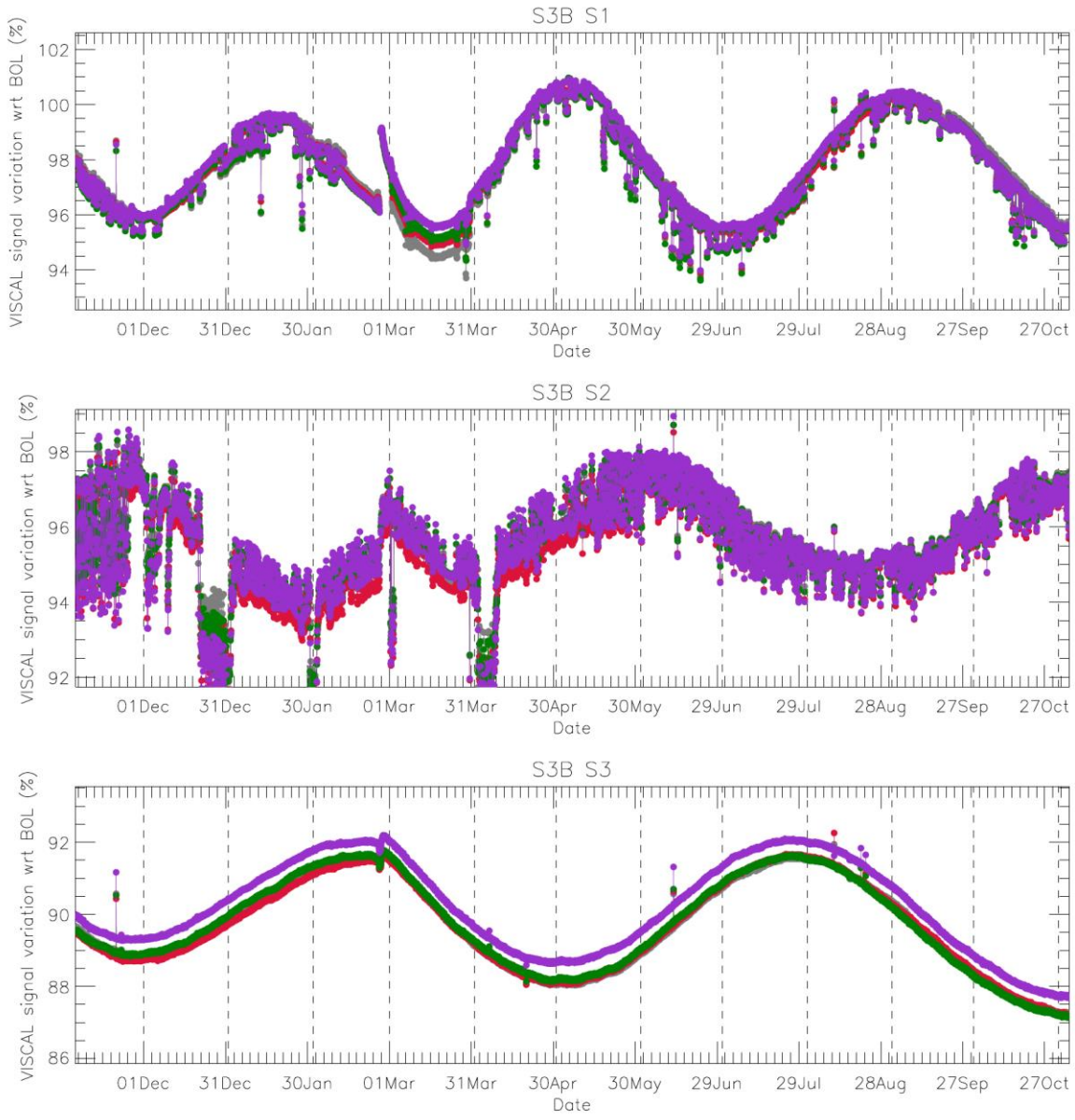

Figure 18: Variation of the radiometric gain derived from the VISCAL signals for SLSTR-B VIS channels for the past year (nadir view). Different colours represent different detectors. The vertical dashed lines indicate the start of each month.

SWIR VISCAL signal variation over the past year

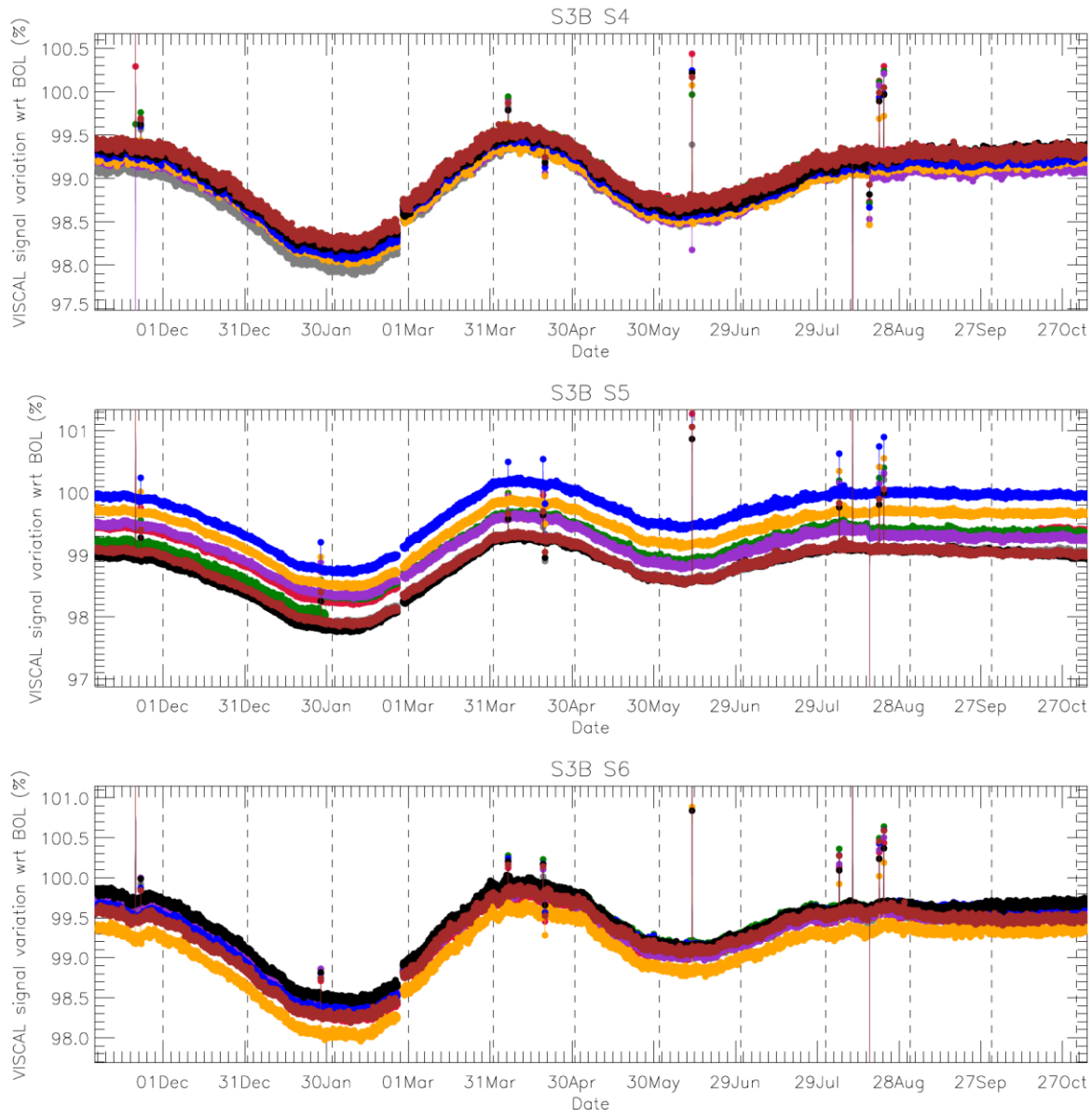

Figure 19: Variation of the radiometric gain derived from the VISCAL signals for SLSTR-B SWIR channels for the past year (nadir view). Different colours represent different detectors. The vertical dashed lines indicate the start of each month.

5 Level-1 product validation

Level-1 product quality is assessed in terms of radiometric and geometric accuracy

The Level-1 image quality is assessed when data are available at the MPC. For example, by combining all granules over one day into a single combined image. The S3A and S3B satellites are configured to be 140 degrees out of phase in order to observe complimentary portions of the earth. Figure 20 shows an example combined SLSTR-A/SLSTR-B image for the visible channels on 31st of October 2023 (daytime only).

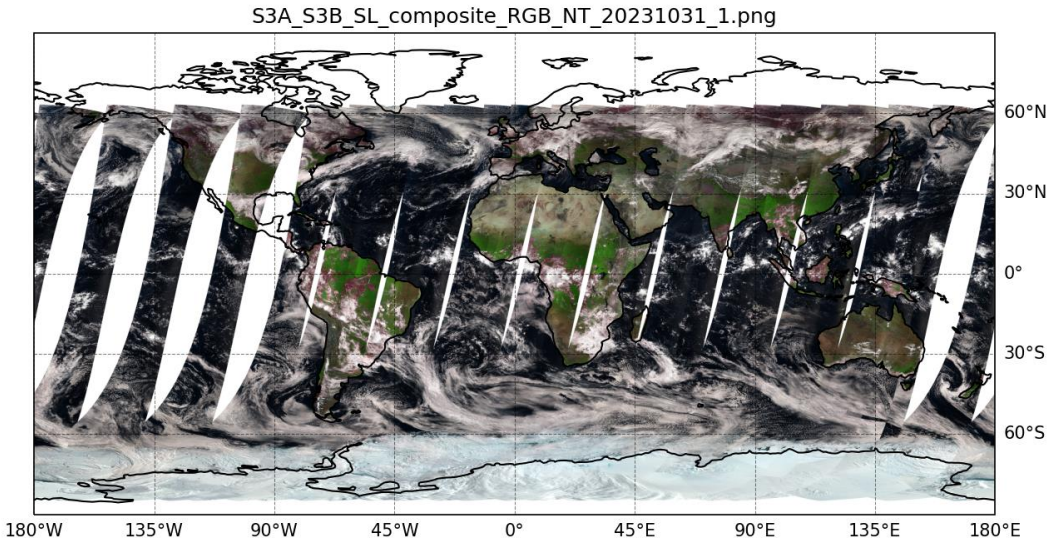

Figure 20: Daytime combined SLSTR-A and SLSTR-B Level-1 image for visible channels on 31st of October 2023.

5.1 Level-1 TIR Radiometric Validation

S3_MR_1000 Relative radiometric accuracy: Sentinel-3 infrared channels shall have a relative radiometric accuracy of <0.08K (threshold) with a goal of 0.05 K over a range of 210-350 K expressed as NEDT traceable to international reference standards.

The absolute radiometric calibration of the IR channels is being validated by EUMETSAT using comparisons against IASI-A and B (Tomazic et al 2018). These results confirmed very good performance with almost no bias (< 0.1 K) for channels S8 and S9 in the nadir view over the temperature range 220 – 280 K.

5.2 Level- 1 VIS SWIR Radiometric Validation

A3_MR_1010 Absolution radiometric accuracy: Sentinel-3 VIS reflectance at TO shall have an absolute radiometric accuracy goal of < 2% with reference to the sun for the 400-900 nm wavebands and <5% with reference to the sun for wavebands >900 nm traceable to international reference standards.

Validation of the VIS/SWIR radiometric measurements is performed by various methods to establish the magnitude of any calibration offset. Some activities are routinely performed each month and reported here, and some are less regular and reported in the annual data quality reports.

The results of these different methods have been collated and have been found to agree that there is a calibration offset present in the VIS/SWIR radiances. It is recommended therefore that users apply an offset in-line with the values presented in Table 7. These offsets are stable and apply to the entire mission. Note that uncertainty estimates are at k=1.

Nadir View	S1	S2	S3	S5	S6
Correction	0.97	0.98	0.98	1.11	1.13
Uncertainty	0.03	0.02	0.02	0.02	0.02
Oblique View	**S1**	**S2**	**S3**	**S5**	**S6**
Correction	0.94	0.95	0.95	1.04	1.07
Uncertainty	0.05	0.03	0.03	0.03	0.05

Table 7. The recommended corrections that should be applied to SLSTR-A and SLSTR-B VIS, SWIR channels.

5.2.1 Radiometric validation with DIMITRI

5.2.1.1 Verification and Validation over PICS

1. The ingestion of the available L1-RBT-NT products from SLSTR-A and SLSTR-B over the 6 desert CalVal-sites (Algeria3 & 5, Libya 1 & 4 and Mauritania 1 & 2) has been performed until the **mid October 2023**.
2. The results are consistent over all the six used PICS sites (Figure 21 and Figure 22). Both sensors show a good stability over the analysed period over VNIR bands for both NADIR & OBLIQUE views, with slight positive trend.
3. The temporal average over the period **1st January 2023- mid-October 2023** of the elementary ratios (observed reflectance to the simulated one) for **SLSTR-A** and **SLSTR-B** show gain values between 3-6% (NADIR) and 6-9% (OBLIQUE) over the VNIR bands S1-S3 (Figure 23).

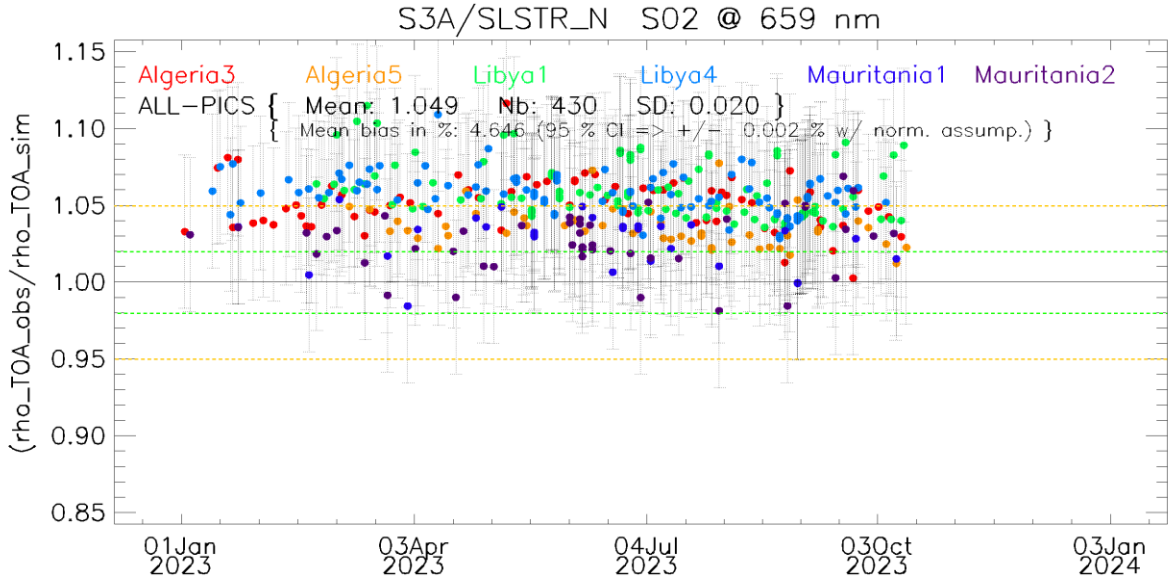
S3A/SLSTR_N S02 @ 659 nm
Algeria3
Algeria5
Libya1
Libya4
Mauritania1
Mauritania2
ALL−PICS { Mean: 1.049 Nb: 430 SD: 0.020 }
{ Mean bias in %: 4.646 (95 % CI => +/− 0.002 % w/ norm. assump.) }
(rho_TOA_obs/rho_TOA_sim
1.15
1.10
1.05
1.00
0.95
0.90
0.85
01Jan 2023
03Apr 2023
04Jul 2023
03Oct 2023
03Jan 2024

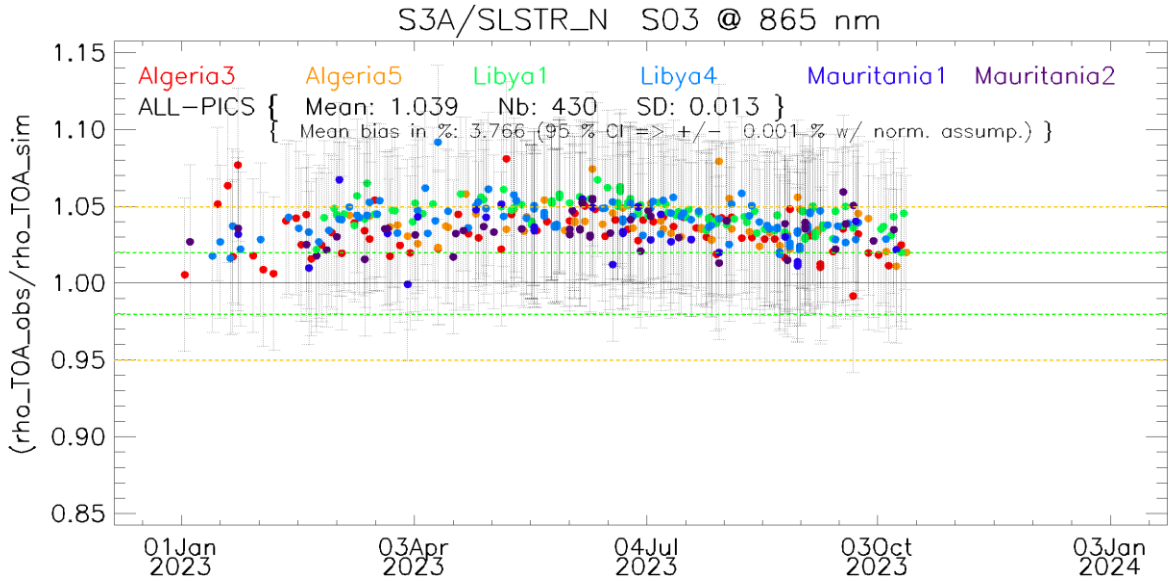
S3A/SLSTR_N S03 @ 865 nm
Algeria3
Algeria5
Libya1
Libya4
Mauritania1
Mauritania2
ALL−PICS { Mean: 1.039 Nb: 430 SD: 0.013 }
{ Mean bias in %: 3.766 (95 % CI => +/− 0.001 % w/ norm. assump.) }
(rho_TOA_obs/rho_TOA_sim
1.15
1.10
1.05
1.00
0.95
0.90
0.85
01Jan 2023
03Apr 2023
04Jul 2023
03Oct 2023
03Jan 2024

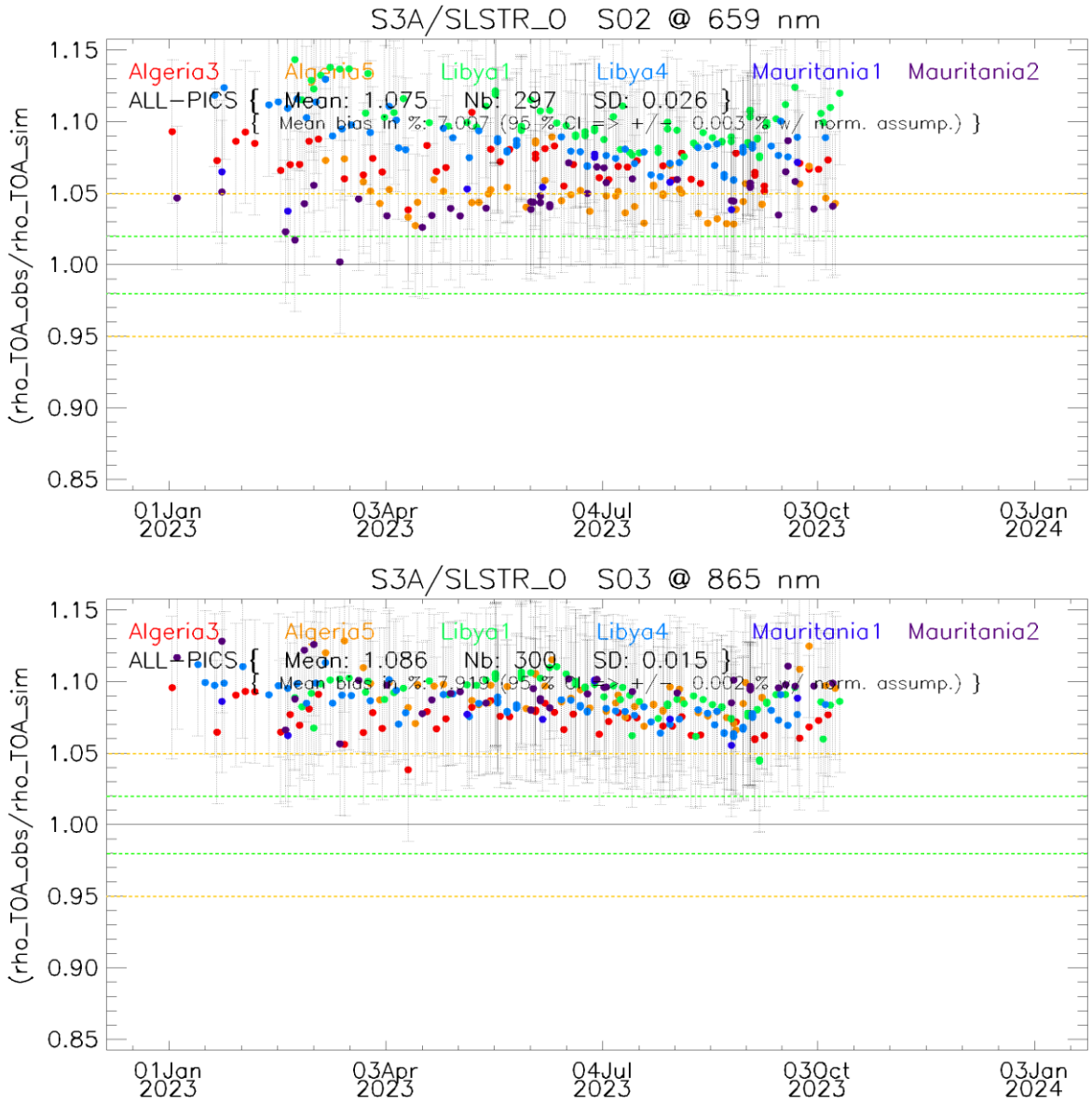

Figure 21: Time-series of the elementary ratios (observed/simulated) signal from SLSTR-A for (top to bottom) bands S02 and S03 (Nadir & Oblique views) respectively over January 2023- mid-October 2023 from the six PICS Cal/Val sites. Dashed-green and orange lines indicate the 2% and 5% respectively. Error bars indicate the desert methodology uncertainty.

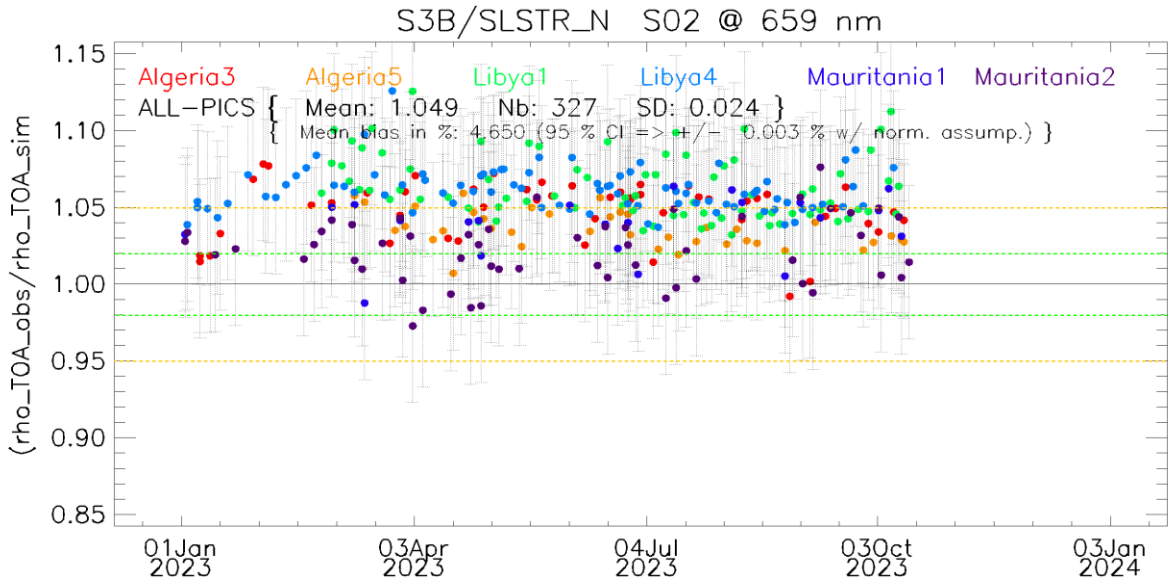
S3B/SLSTR_N S02 @ 659 nm
Algeria3
Algeria5
Libya1
Libya4
Mauritania1
Mauritania2
ALL-PICS { Mean: 1.049 Nb: 327 SD: 0.024 }
{ Mean bias in %: 4.650 (95 % CI => +/- 0.003 % w/ norm. assump.) }
(rho_TOA_obs/rho_TOA_sim
1.15
1.10
1.05
1.00
0.95
0.90
0.85
01Jan 2023
03Apr 2023
04Jul 2023
03Oct 2023
03Jan 2024

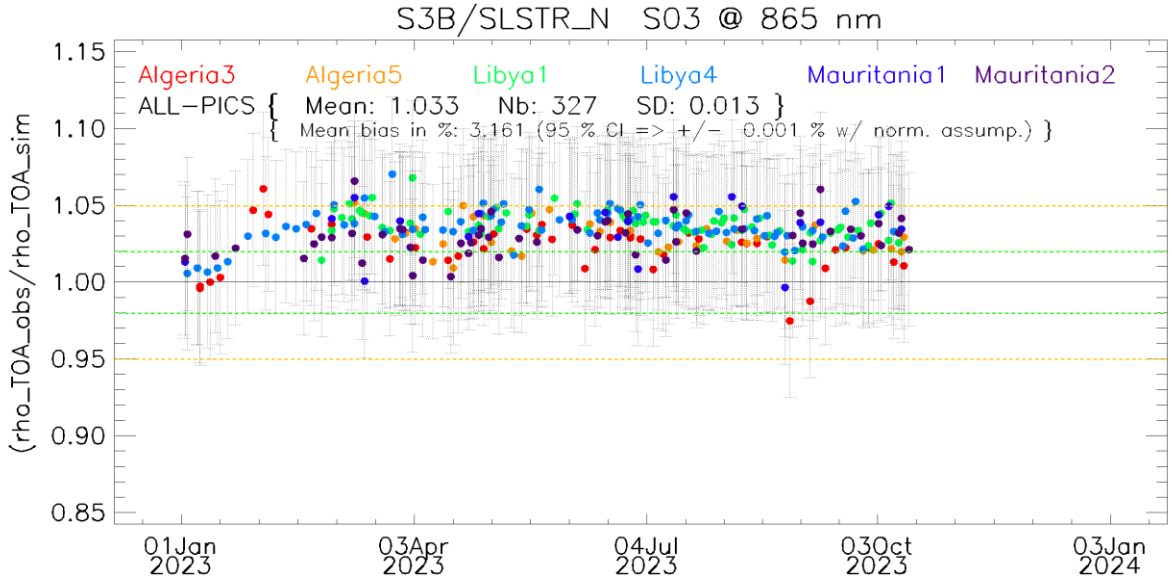
S3B/SLSTR_N S03 @ 865 nm
Algeria3
Algeria5
Libya1
Libya4
Mauritania1
Mauritania2
ALL-PICS { Mean: 1.033 Nb: 327 SD: 0.013 }
{ Mean bias in %: 3.161 (95 % CI => +/- 0.001 % w/ norm. assump.) }
(rho_TOA_obs/rho_TOA_sim
1.15
1.10
1.05
1.00
0.95
0.90
0.85
01Jan 2023
03Apr 2023
04Jul 2023
03Oct 2023
03Jan 2024

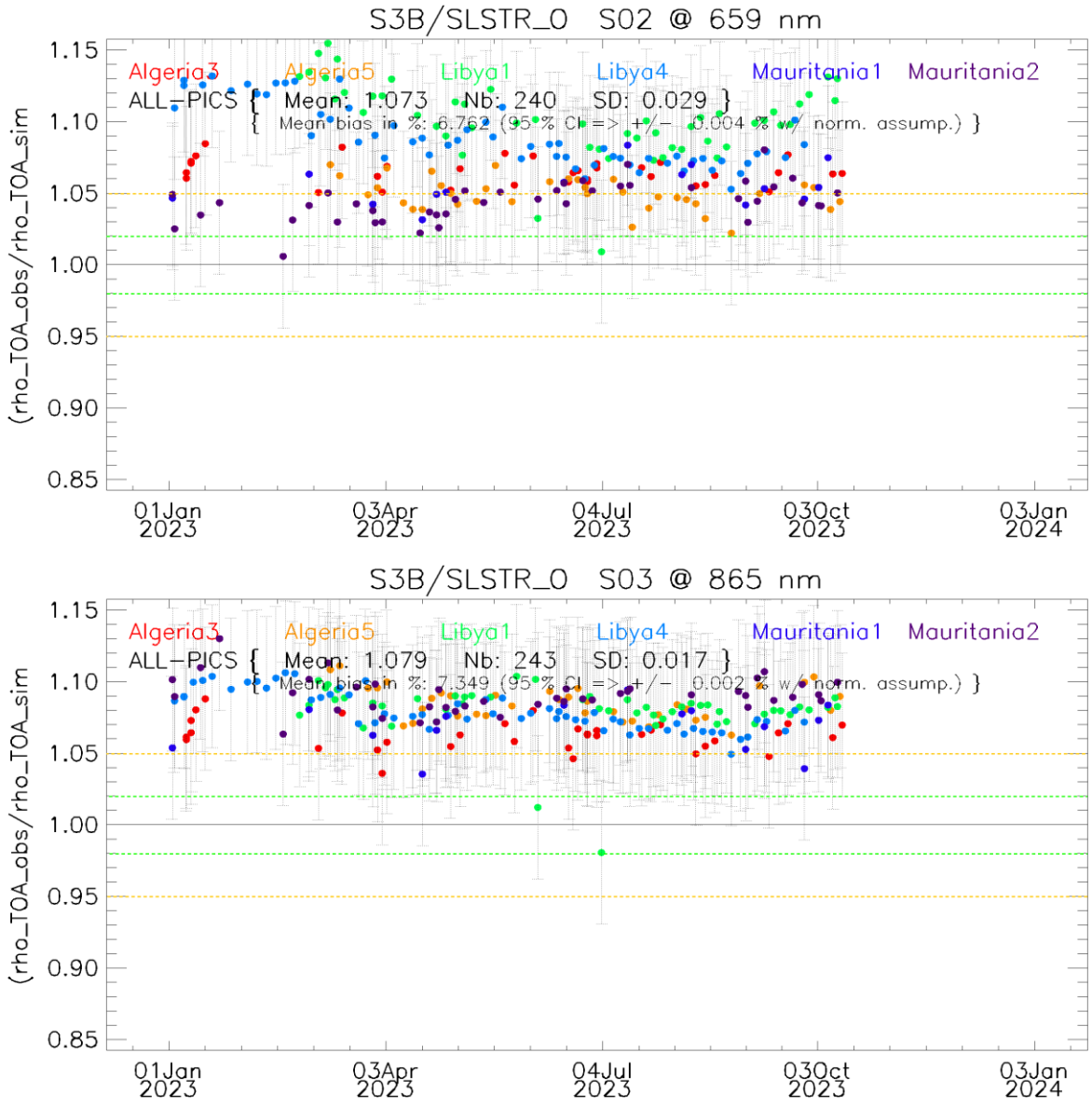

Figure 22: Time-series of the elementary ratios (observed/simulated) signal from SLSTR-B for (top to bottom) bands S02 and S03 (Nadir & Oblique views) respectively over January 2023- mid-October 2023 from the six PICS Cal/Val sites. Dashed-green and orange lines indicate the 2% and 5% respectively. Error bars indicate the desert methodology uncertainty.

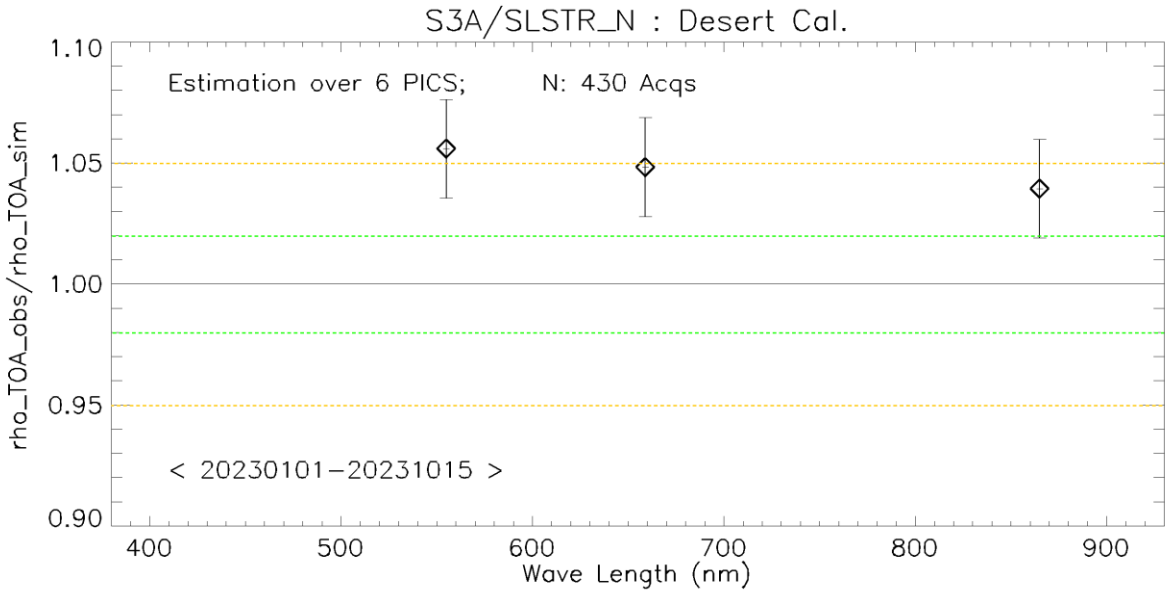
S3A/SLSTR_N : Desert Cal.
Estimation over 6 PICS;
N: 430 Acqs
< 20230101-20231015 >
rho_TOA_obs/rho_TOA_sim
Wave Length (nm)
1.10
1.05
1.00
0.95
0.90
400
500
600
700
800
900

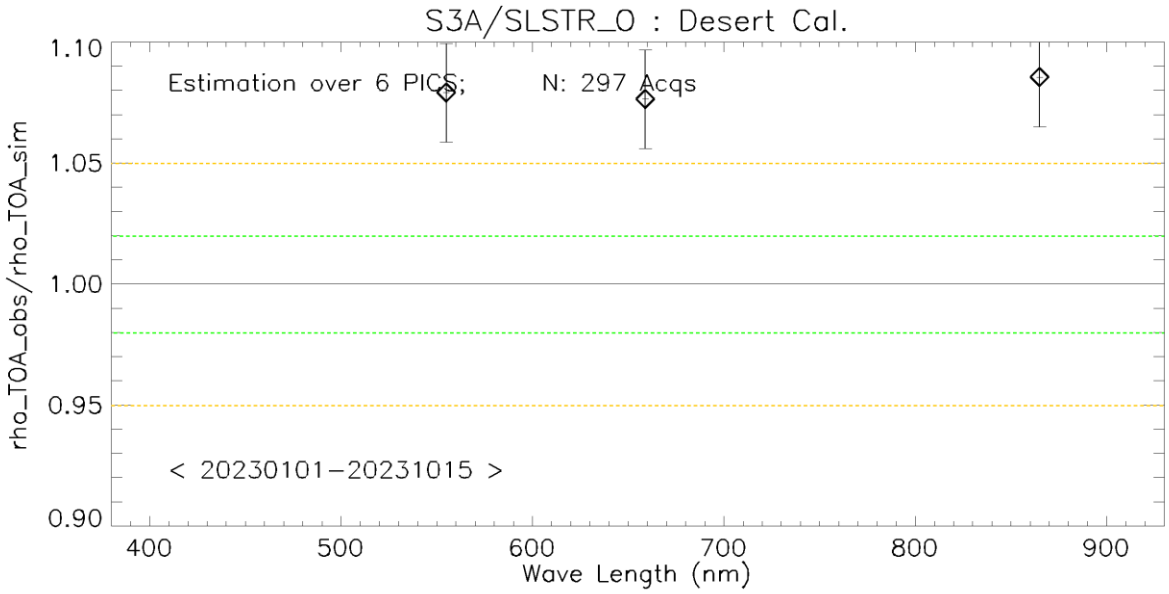
S3A/SLSTR_O : Desert Cal.
Estimation over 6 PICS;
N: 297 Acqs
< 20230101-20231015 >
rho_TOA_obs/rho_TOA_sim
Wave Length (nm)
1.10
1.05
1.00
0.95
0.90
400
500
600
700
800
900

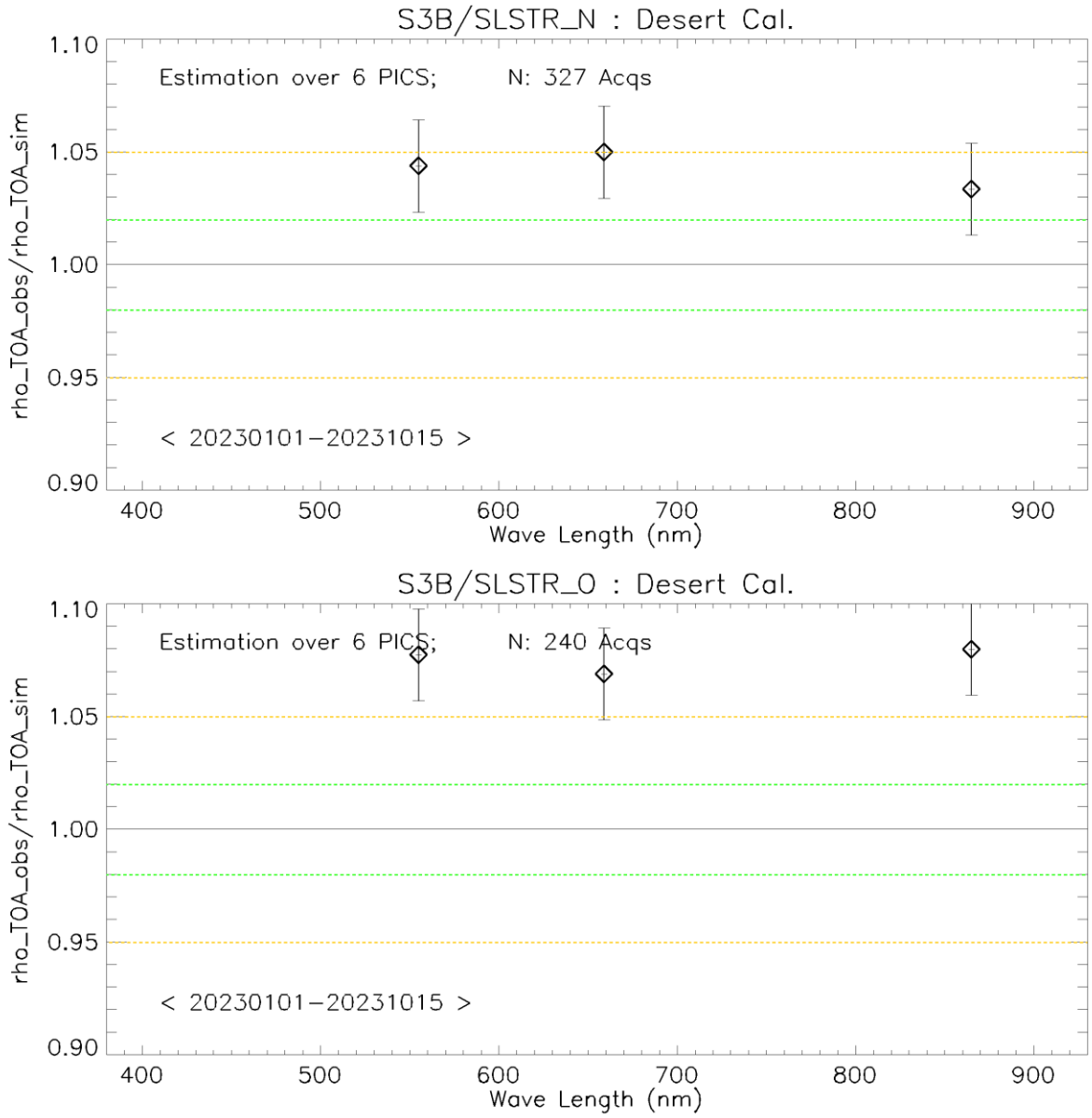

Figure 23: The estimated gain values for SLSTR-A and SLSTR-B (top to bottom) Nadir & Oblique views respectively over the 6 PICS sites identified by CEOS over the period January 2023- mid-October 2023 as a function of wavelength. Dashed-green and orange lines indicate the 2% and 5% respectively. Error bars indicate the desert methodology uncertainty.

5.2.1.2 Validation over Rayleigh

Rayleigh method has been performed from the available mini-files over the period **January 2022- mid-October 2023** for SLSTR-A and SLSTR-B. The gain coefficients of both sensors are consistent with the previous results (Figure 24).

5.2.1.3 Validation over Glint

Glint calibration method has been performed over the period **January 2022- mid-October 2023** for both SLSTR-A and SLSTR-B. The gain coefficients of both sensors are consistent with the previous results over the Nadir view (Figure 24).

5.2.1.4 Validation results synthesis

The results synthesis displayed below on (Figure 24).

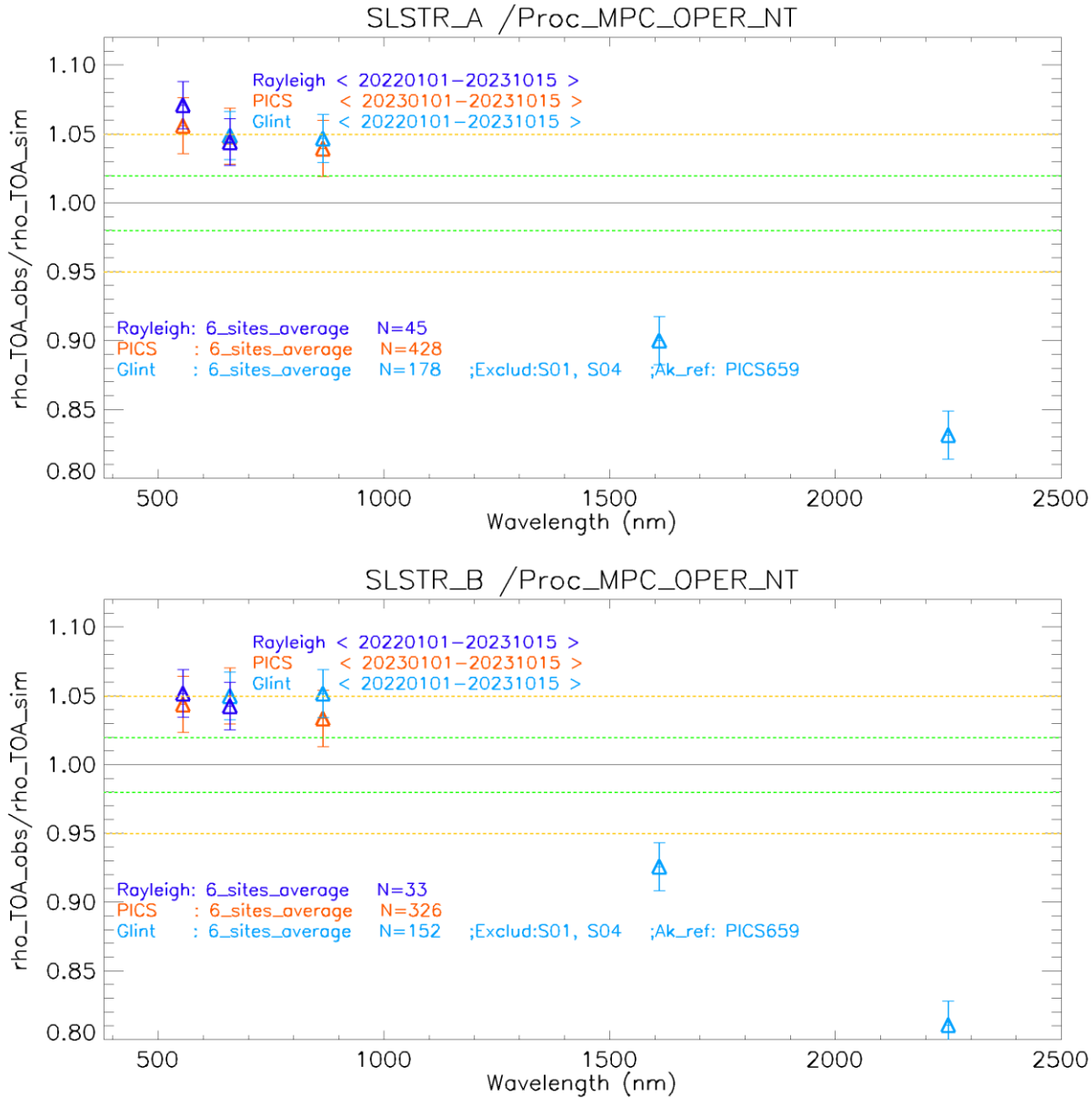

Figure 24: The estimated gain values for SLSTR-A and SLSTR-B (Nadir view) from Glint and Rayleigh methods over the period Jan 2022—mid-October 2023 and PICS method over the period Jan 2023—mid-October 2023 as a function of wavelength. We use the gain value of S02 from Desert-PICS method as reference gain for Glint method. Dashed-green and orange lines indicate the 2% and 5% respectively. Error bars indicate the method uncertainties.

5.2.1.5 Cross-mission Intercomparison over PICS:

X-mission Intercomparison between SLSTR-A, SLSTR-B, MERIS, MSI-A, MSI-B, OLCI-A and OLCI-B has been performed over the 6 PICS-test-sites. Figure 25 shows the estimated gain over different time-series for different sensors over PICS. The spectral bands with significant absorption of water vapor and O2 are excluded. OLCI-A, SLSTR-A and SLSTR-B seem to have higher gain wrt the other sensors of about 1-4% over VNIR spectral range.

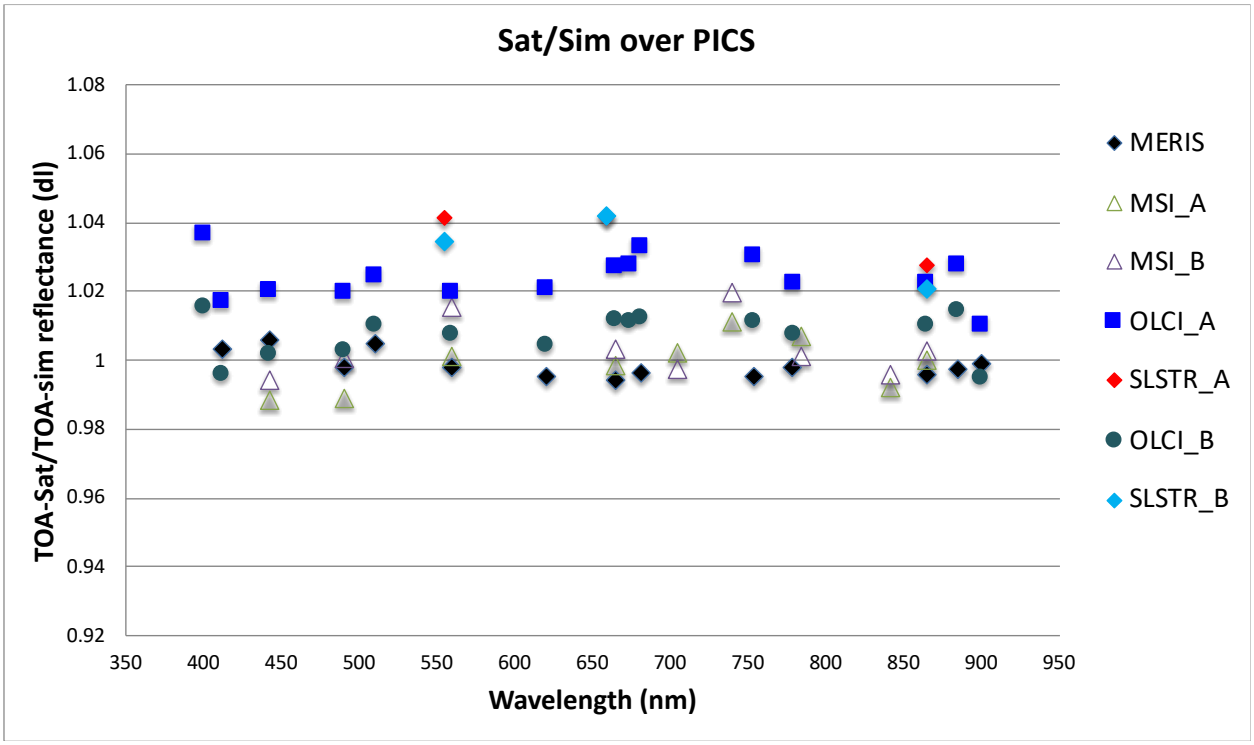

Figure 25: Ratio of observed TOA reflectance to simulated one for (black) MERIS, (pale-green) S2A/MSI, (white) S2B/MSI, (blue) S3A/OLCI, (green) S3B/OLCI, (red) S3A/SLSTR-NADIR, and (cyan) S3B/SLSTR-NADIR averaged over the six PICS test sites as a function of wavelength.

5.3 Level-1 Geometric Validation

S3_MR_1090 Geolocation accuracy: Improved geo-location accuracy is possible when using ground control points and Sentinel-3 shall be designed to ensure a geolocation accuracy of better than 0.5rm of the spatial resolution of the optical sensor when using ground control points.

S3_MR_1100 Inter channel co-registration. The inter channel spatial co-registration for Sentinel-3 visible measurements shall be < 0.5 of the spatial resolution of the sensor over the full spectral range (goal of 0.3 of the spatial resolution of the sensor)

S3_MR_1100 Inter channel co-registration: The inter channel spatial co-registration for Sentinel-3 SWIR and TIR measurements shall be sufficient to allow these channels to be co registered with visible channels at higher spatial resolution data.

Regular monitoring using the GeoCal Tool implemented at the MPC is normally carried out. On average, the geolocation accuracy of the VIS-SWIR channels meets requirements for SLSTR-A and SLSTR-B.

GeoCal is a tool that monitors the geolocation performance in Level-1 images by correlation of the images with reference features containing ground control points (GCP). Each Level-1 granule typically contains several hundred GCPs if over land, which are filtered based on signal-to-noise to obtain a daily average in the across and along track directions.

The geolocation uncertainty is stable and within requirements during the reporting period.

5.3.1 SLSTR-A

The results for October 2023 are plotted in Figure 26 for SLSTR-A, giving the average positional offsets in kilometres for Nadir and Oblique views.

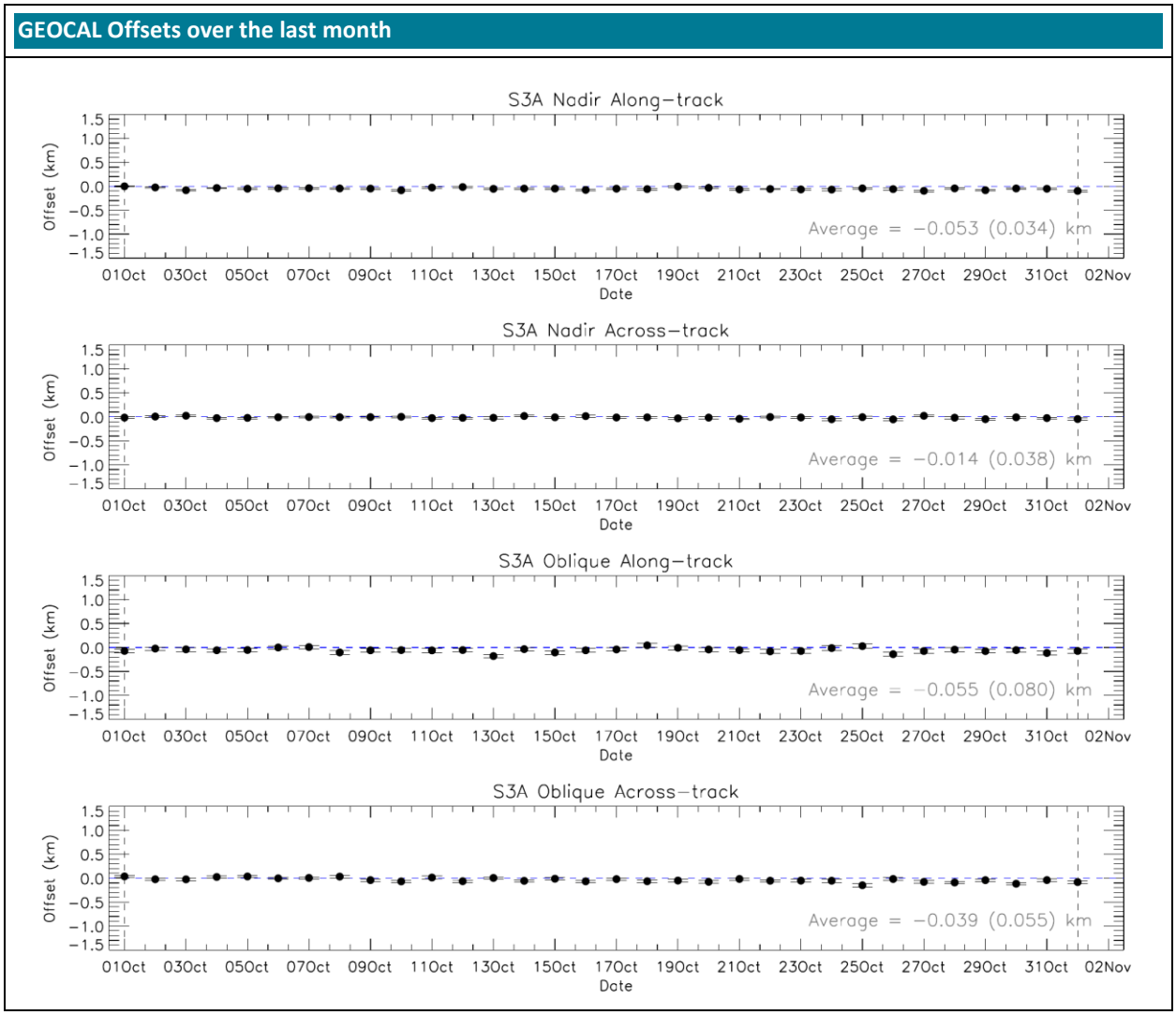

Figure 26: SLSTR-A daily offset results in km from the GeoCal Tool analysis for Nadir along- and across-track (top two plots) and Oblique along- and across-track (bottom two plots) for October 2023. The error bars show the standard deviation.

5.3.2 SLSTR-B

The results for October 2023 are plotted in Figure 27 for SLSTR-B, giving the average positional offsets in kilometres for Nadir and Oblique views.

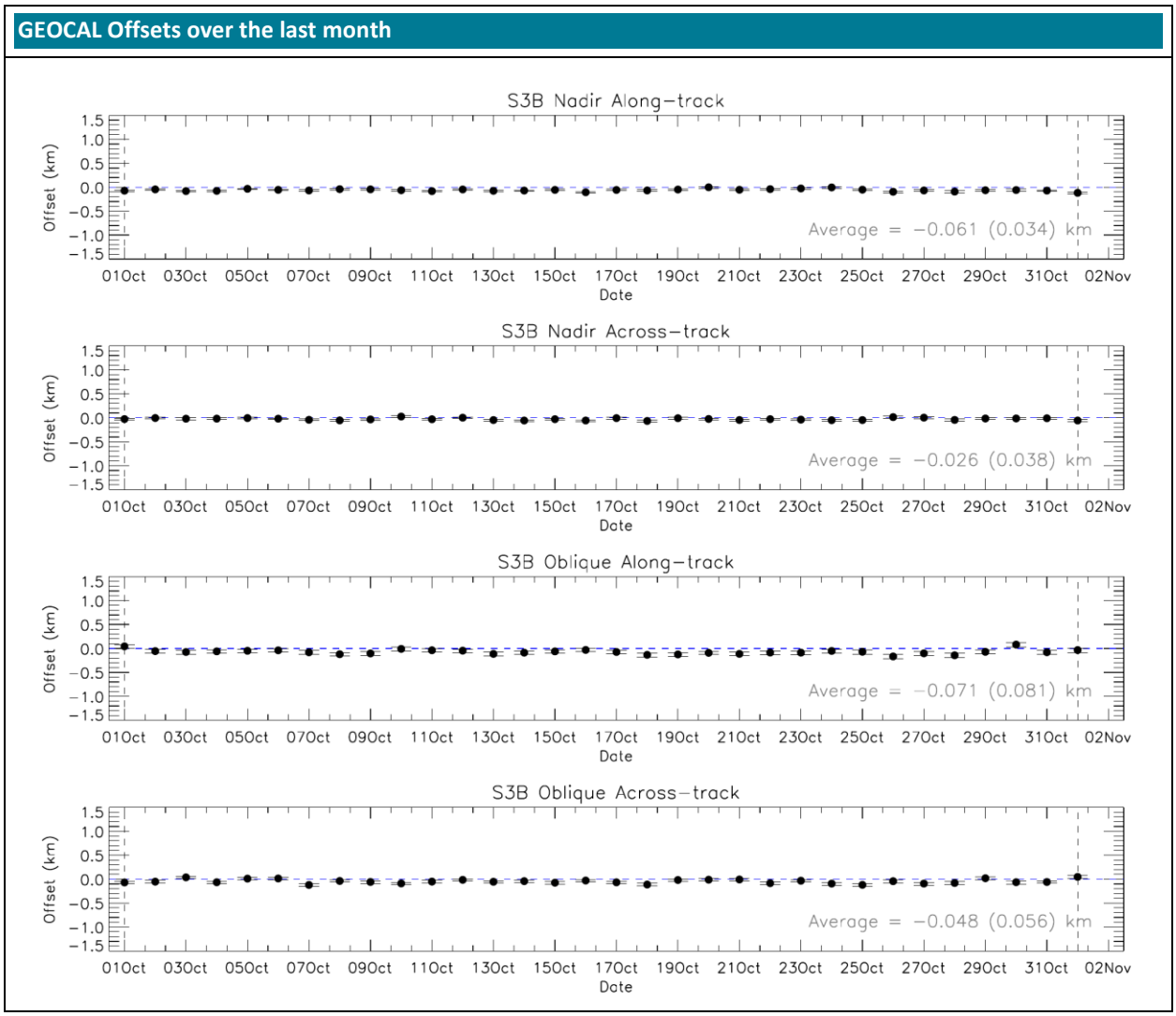

Figure 27: SLSTR-B daily offset results in km from the GeoCal Tool analysis for Nadir along- and across-track (top two plots) and Oblique along- and across-track (bottom two plots) for October 2023. The error bars show the standard deviation.

6 Level 2 LST validation

Level 2 Land Surface Temperature products have been validated against *in situ* observations (Category-A validation) from eight "Gold Standard" Stations. The different categories of validation are first described in the LST Validation Protocol (Schneider et al., 2012) and reinforced in the CEOS WGCV-LPV Land Surface Temperature Product Validation Best Practice Protocol (Guillevic et al., 2017). In all cases it is the NTC products that are validated, and the Probabilistic cloud masking implementation is used for all cloud masking. Both S3A and S3B L2 products are produced with the updated LST coefficients following the operational release on 25th February 2019. In each case the latest temporal interpolation for the probabilistic cloud mask is applied following the L1 operational release on 15th January 2020. The updated cloud coefficients ADF was applied on 23rd October 2020.

6.1 Category-A validation

Category-A validation uses a comparison of satellite-retrieved LST with *in situ* measurements collected from radiometers sited at a number of stations spread across the Earth, for which the highest-quality validation can be achieved. Here we concentrate on twelve "Gold Standard" stations which are installed with well-calibrated instrumentation: twelve from the SURFRAD network (Bondville, Illinois; Desert Rock, Nevada; Fort Peck, Montana; Goodwin Creek, Mississippi; Penn State University, Pennsylvania; Sioux Fall, South Dakota; Table Mountain, Colorado); two from the ARM network (Southern Great Plains, Oklahoma; Barrow, Alaska); and three from the USCRN network (Williams, Arizona; Des Moines, Iowa; Manhatten, Kansas).

For the SURFRAD field pyrgeometers the uncertainty is estimated to be ±5 Wm-2 (Augustine and Dutton, 2013). For ARM, the uncertainty of the measured brightness temperatures was set to ±0.5 K for Southern Great Plains (Morris, 2006), and for North Slopes Alaska the uncertainty of the IR radiance data was set to ±4 Wm-2 (Stoffel, 2006). For the USCRN network, which uses Apogee SI-121s the uncertainty is set as the manufacturers estimate of ±0.2 K.

The results can be summarised as follows (accuracy is used as the metric rather than uncertainty as this is then a straight comparison with mission requirements):

Table 8: Average absolute accuracy in K of the SL_2_LST product with respect to Gold Standard stations for Q3 2023.

Satellite	Day	Night
S3A	1.5	1.2
S3B	1.7	1.2

For both SLSTR-A and SLSTR-B both the daytime and night-time absolute accuracies (which are derived from the absolute values of all the mean biases from the individual stations) are greater than the mission requirement of 1K, but driven by larger biases at some sites. The main impact on accuracy and precision is driven by any errors in the cloud masking, but also higher temperatures. The recommendation would be to assess whether an improvement could be made with the retrieval coefficients particularly during the day for higher temperatures.

SLSTR-A	SLSTR-B
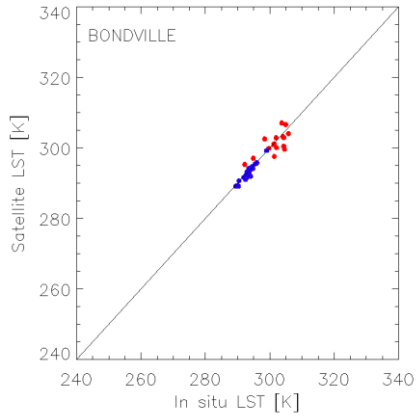	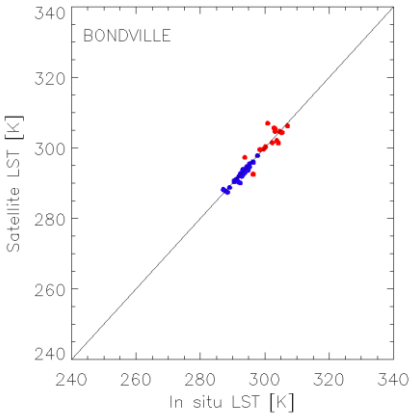
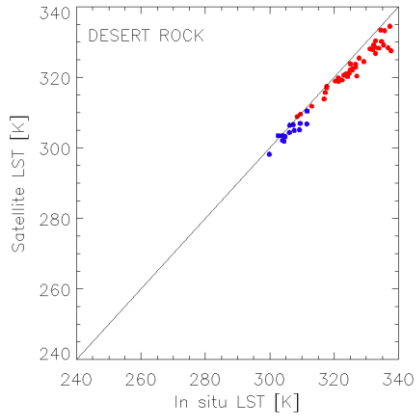	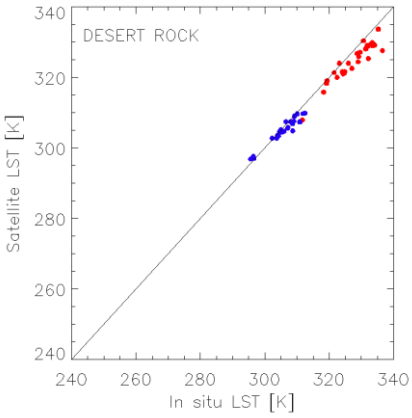
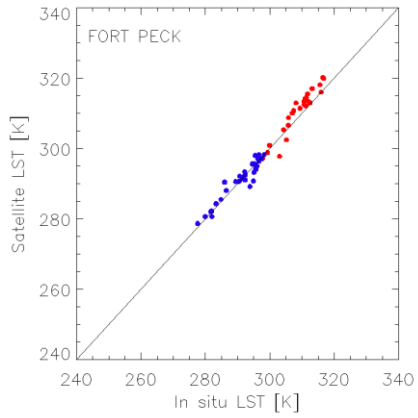	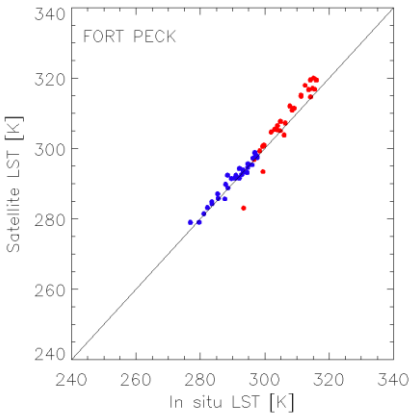

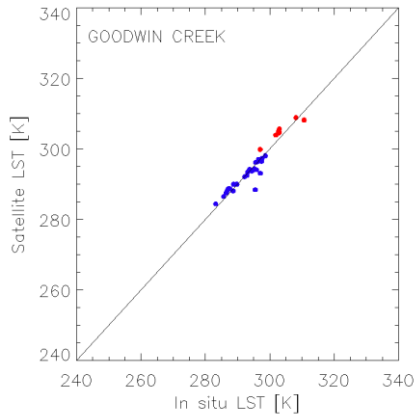
GOODWIN CREEK
Satellite LST [K]
In situ LST [K]
240
260
280
300
320
340

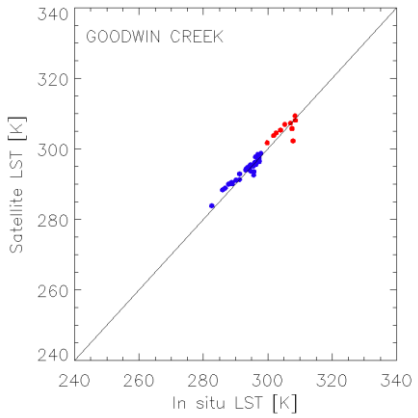
GOODWIN CREEK
Satellite LST [K]
In situ LST [K]
240
260
280
300
320
340

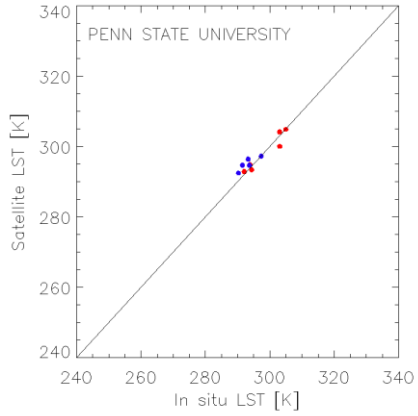
PENN STATE UNIVERSITY
Satellite LST [K]
In situ LST [K]
240
260
280
300
320
340

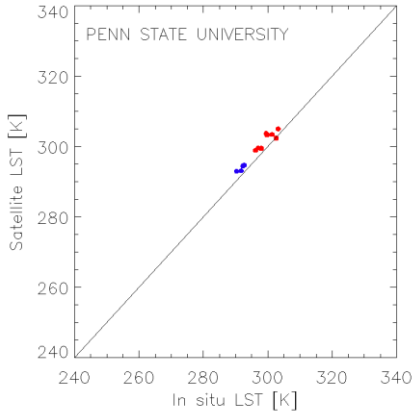
PENN STATE UNIVERSITY
Satellite LST [K]
In situ LST [K]
240
260
280
300
320
340

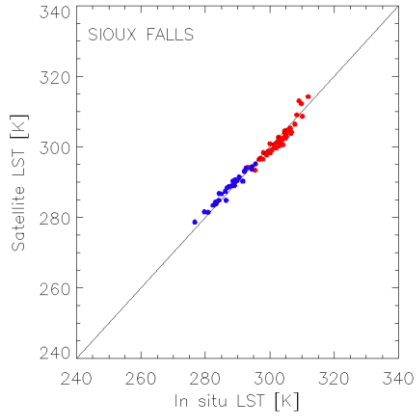
SIOUX FALLS
Satellite LST [K]
In situ LST [K]
240
260
280
300
320
340

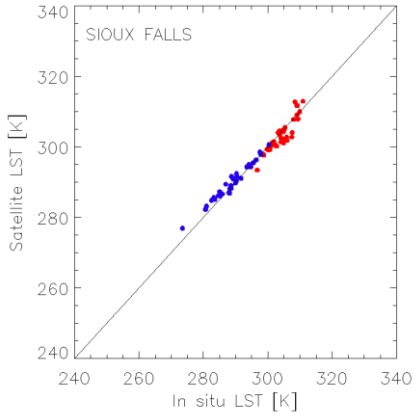
SIOUX FALLS
Satellite LST [K]
In situ LST [K]
240
260
280
300
320
340

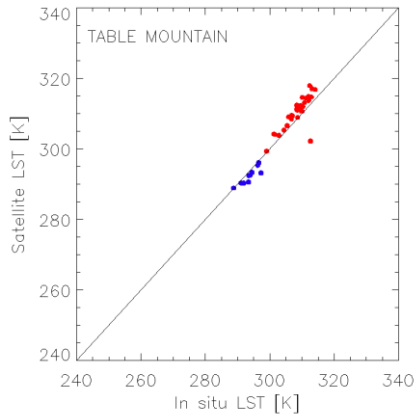
TABLE MOUNTAIN
Satellite LST [K]
In situ LST [K]
240
260
280
300
320
340

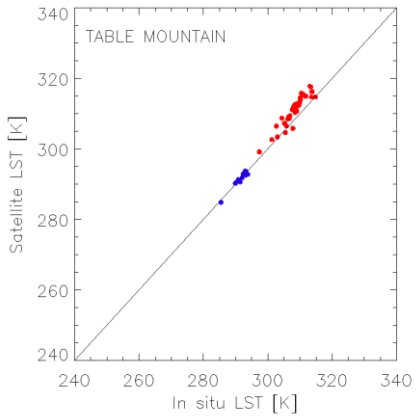
TABLE MOUNTAIN
Satellite LST [K]
In situ LST [K]
240
260
280
300
320
340

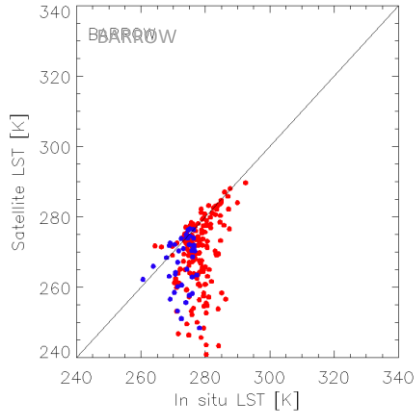
BARROW
Satellite LST [K]
In situ LST [K]
240
260
280
300
320
340

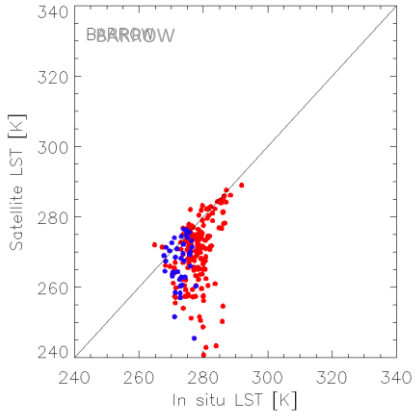
BARROW
Satellite LST [K]
In situ LST [K]
240
260
280
300
320
340

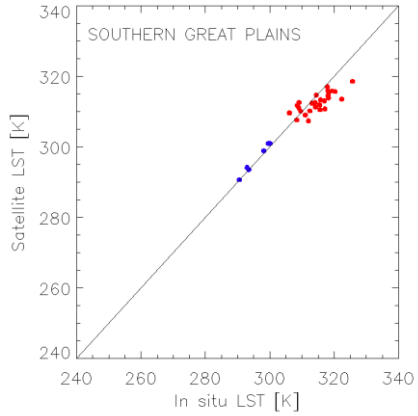
SOUTHERN GREAT PLAINS
Satellite LST [K]
In situ LST [K]
240
260
280
300
320
340

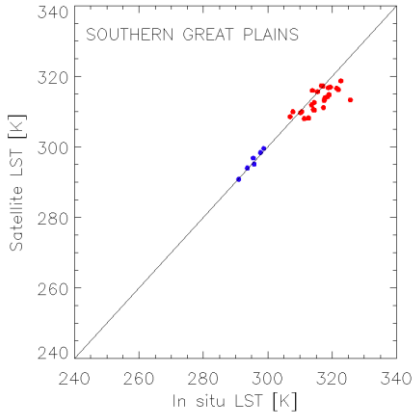
SOUTHERN GREAT PLAINS
Satellite LST [K]
In situ LST [K]
240
260
280
300
320
340

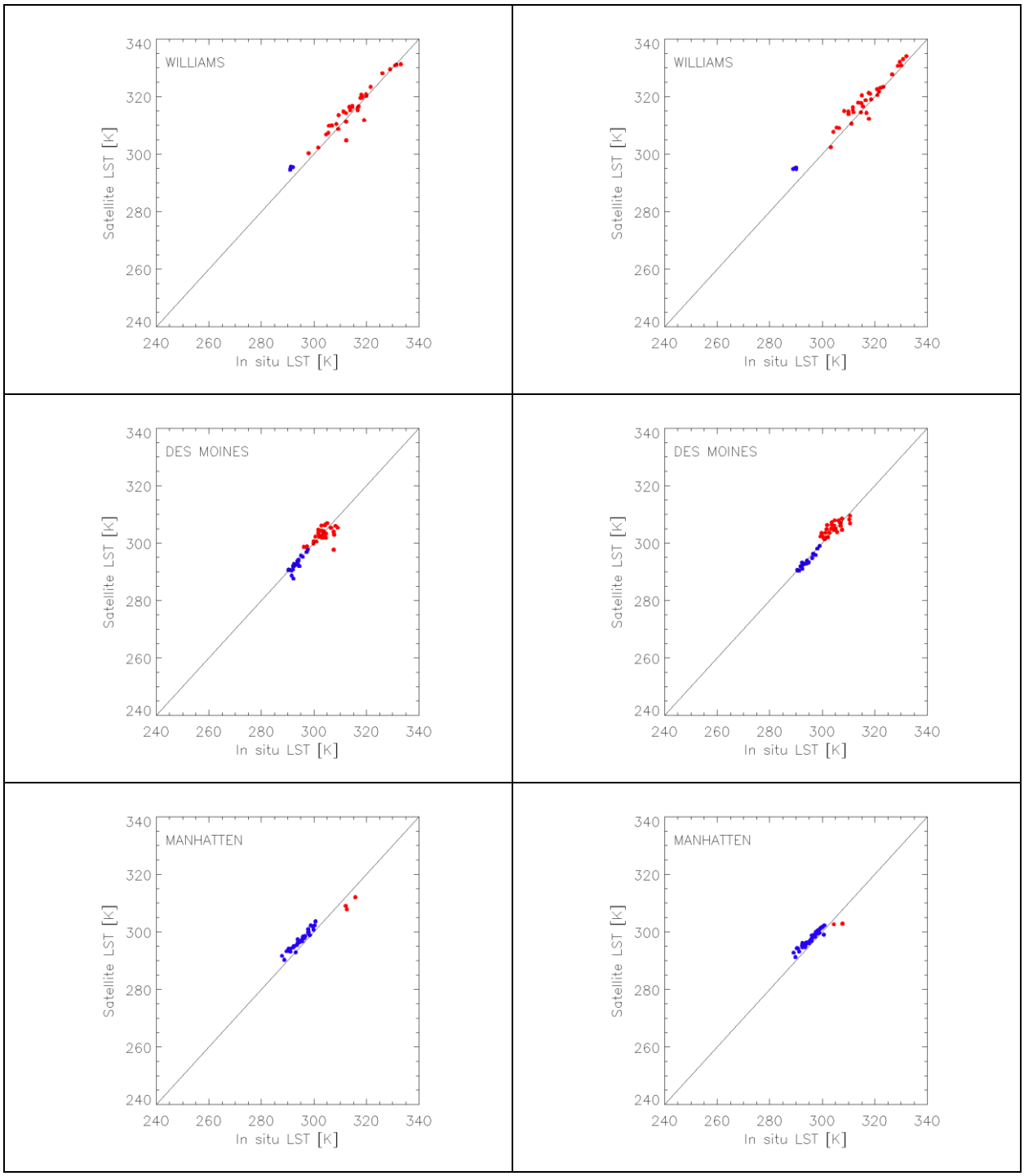

Figure 28: Validation of the SL_2_LST product in Q3 2023 for SLSTR-A (left) and SLSTR-B (right) at twelve Gold Standard in situ stations of the SURFRAD network plus two Gold Standard station from the ARM network. The matchups are split between daytime (red) and night-time (blue).

As with past cycles cloud has reduced the number of matchups per station to single figures for most stations during day or night, with some missing statistics entirely. It is therefore challenging to determine robust statistics. The cumulative statistics are presented in each Annual Report. Nonetheless, it can be seen that overall the matchups are in general close to the 1:1 line with few outliers. There is a small systematic bias evident at some stations, particularly during the day, which may indicate an update to the retrieval coefficients may be worth exploring. Some cloud over-masking (night-time) and under-masking (daytime) appears for some of the sites, and may be worth exploring whether the cloud coefficients need further fine tuning. This is certainly the case for the Barrow site.

6.2 Category-C validation

Category-C validation uses inter-comparisons with similar LST products from other sources such as other satellite sensors, which give important quality information with respect to spatial patterns in LST deviations. Here we compare the SL_2_LST product from both SLSTR-A and SLSTR-B with the operational SEVIRI L2 product available from the LSA SAF. The typical uncertainty of the SEVIRI L2 product ranges between ~1 K over much of Africa and ~3 K over the deserts. The results can be summarised:

Table 9: Median differences in K from the intercomparison of the SL_2_LST product with respect to the operational LSA SAF SEVIRI LST product for December 2022

Continent	SLSTR-A		SLSTR-B	
	Day	Night	Day	Night
Africa	-0.1	-0.1	-0.1	-0.1
Europe	1.1	1.3	1.2	1.3

For both Africa and Europe, the median differences across the continent for both SLSTR-A and SLSTR-B are relatively small, with very few locations with larger differences. The median is used to minimise the impact of any outliers. This is the same for both SLSTR-A and SLSTR-B and is primarily driven by differences in viewing geometry between the SLSTR instruments and SEVIRI and is expected, and in agreement with previous studies of polar orbiting matchups with SEVIRI (Ghent et al., 2017; Trigo et al., 2008). Eastern matchups (such as over the Arabian Peninsula and north-eastern Europe) are towards the edge of the SEVIRI disk and therefore represent large viewing angles. At these extreme viewing angles it is expected that SLSTR LST would be increasingly higher than SEVIRI LST, and the SEVIRI uncertainty increases above 3 K at these extreme angles. For both daytime and night-time the differences are mainly < 1K for Africa for both SLSTR-A and SLSTR-B. During daytime differences are over 1K for Europe as a result of increasing differences due to geometry as days get warmer. Differences are not the same as previous cycles for both Europe and Africa which may indicate responses due to changing seasons.

Other analysis can be summarised as follows:

- Differences with respect to biomes tend to be larger during the day for surfaces with more heterogeneity and/or higher solar insolation
- Differences increase for both day and night towards the edge of the SEVIRI disk as the SEVIRI zenith angles become larger

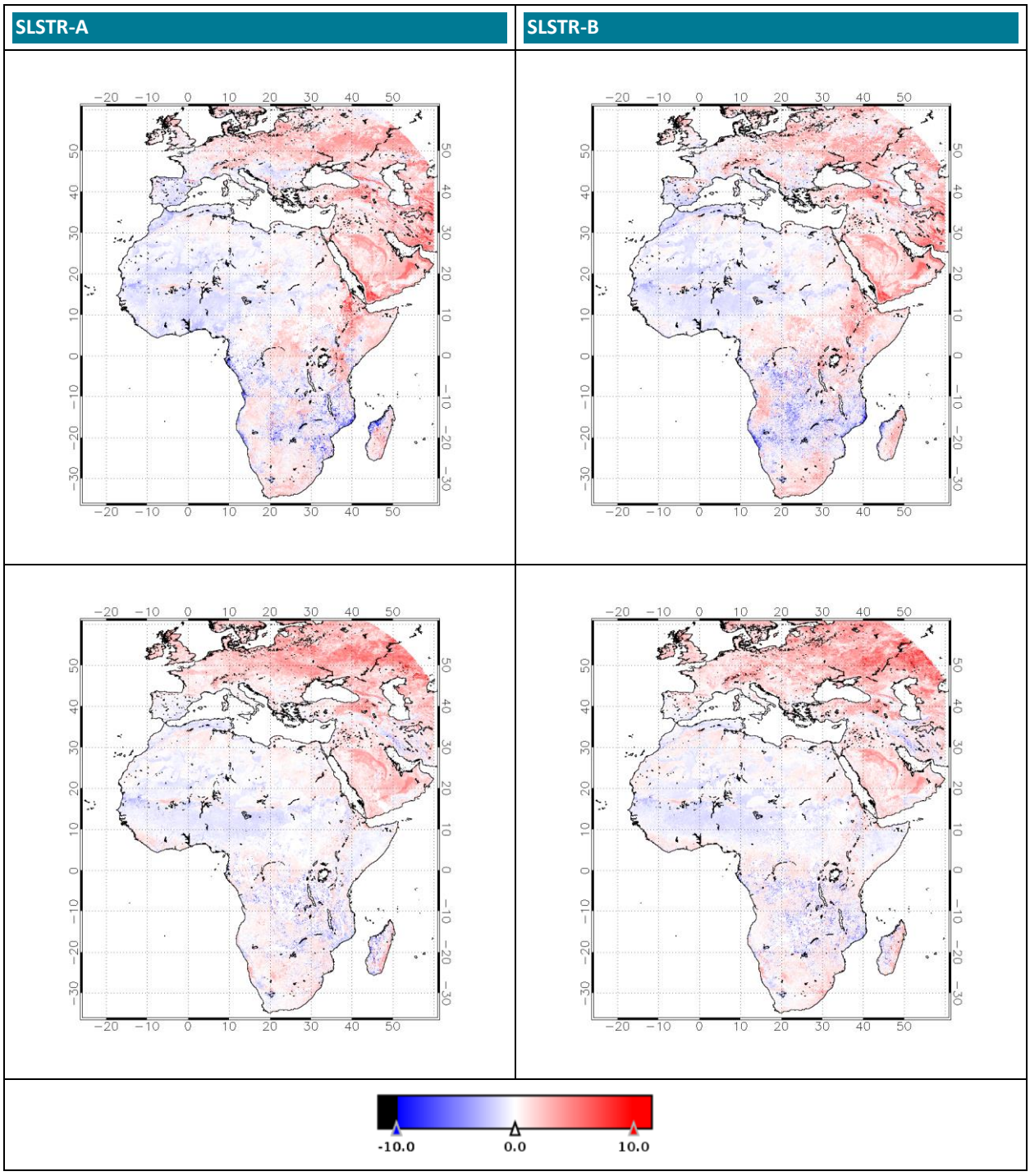

Figure 29: Intercomparison of the SL_2_LST product with respect to the operational LSA SAF SEVIRI LST product for December 2022 for SLSTR-A (left) and SLSTR-B (right). Daytime composites are in the top row and Night-time composites are in the bottom row.

While some of these differences are > 1 K they are all within the corresponding uncertainty of SEVIRI at the pixel-scale (> 2K), and so the **two products can be assessed as being consistent**.

6.3 Level-3C Assessment

To better understand the global product and identify any gross issues Level-3 evaluation is also performed. Here we generate monthly daytime and night-time 0.05° composites of the LST field and corresponding sampling ratios. The sampling ratios are derived as clear_pixels / (clear_pixels + cloudy_pixels).

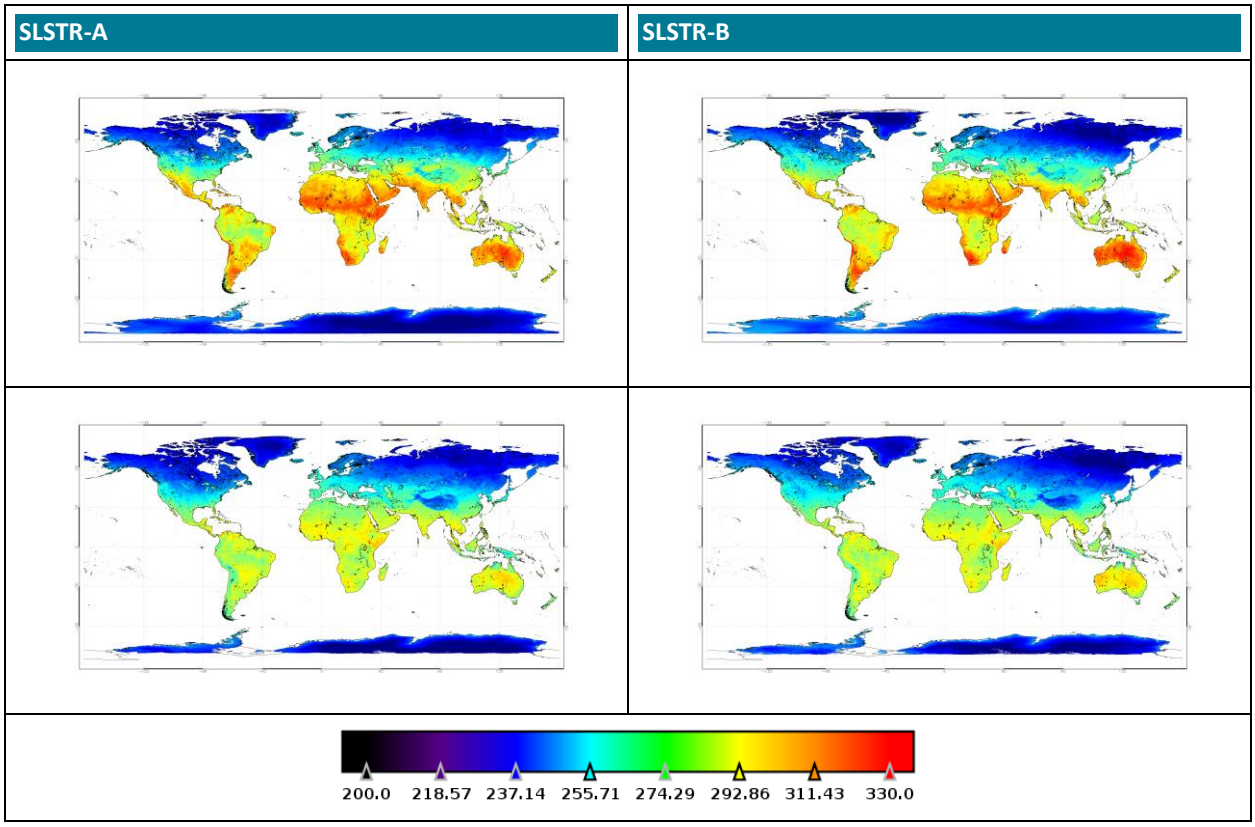

Figure 30: Monthly composites at 0.05° of LST for December 2022 for SLSTR-A (left) and SLSTR-B (right). Daytime composites are in the top row and Night-time composites are in the bottom row.

6.4 References

Augustine, J.A. and Dutton, E.G. (2013). Variability of the surface radiation budget over the United States from 1996 through 2011 from high-quality measurements. Journal of Geophysical Research: Atmospheres 118, 43–53.

Ghent, D. J., Corlett, G. K., Göttsche, F.-M., & Remedios, J. J. (2017). Global land surface temperature from the Along-Track Scanning Radiometers. Journal of Geophysical Research: Atmospheres, 122. https://doi.org/10.1002/2017JD027161

Guillevic, P., Göttsche, F., Nickeson, J., Hulley, G., Ghent, D., Yu, Y., Trigo, I., Hook, S., Sobrino, J.A., Remedios, J., Román, M. & Camacho, F. (2017). Land Surface Temperature Product Validation Best Practice Protocol. Version 1.0. In P. Guillevic, F. Göttsche, J. Nickeson & M. Román (Eds.), Best Practice for Satellite-Derived Land Product Validation (p. 60): Land Product Validation Subgroup (WGCV/CEOS), doi:10.5067/doc/ceoswgcv/lpv/lst.001

Morris, V.R. Infrared Thermometer (IRT) Handbook (ARM TR-015) (2006). Technical report, Atmospheric Radiation Measurement, Climate Research Facility, U. S. Department of Energy.

Schneider, P., Ghent, D., Corlett, G., Prata, F., and Remedies, J. (2012). AATSR validation: LST validation protocol. Internal publication, UL-NILU-ESA-LST-LVP Issue 1 Revision 0, page 1-39. http://lst.nilu.no/Portals/73/Docs/Reports/UL-NILU-ESA-LST-LVP-Issue1-Rev0-1604212.pdf.

Stoffel, T. Ground Radiation (GNDRAD) Handbook (ARM TR-027) (2006). Technical report, Atmospheric Radiation Measurement, Climate Research Facility, U. S. Department of Energy.

Trigo, I. F., Monteiro, I. T., Olesen, F., & Kabsch, E. (2008). An assessment of remotely sensed land surface temperature. Journal of Geophysical Research, 113(D17), D17108. https://doi.org/10.1029/2008JD010035

7 Level 2 FRP validation

7.1 The SLSTR Fire Radiative Power product

The SLSTR FRP NTC product (both SLSTR-A and SLSTR-B) has been released to the public on August 19th, 2020. The current processing baseline for SLSTR-A and SLSTR-B FRP products is FRP_NTC.004.07.00 and was deployed in the Land processing centres on February 28th, 2022, for both SLSTR-A and for SLSTR-B. This baseline is including an updated FRP algorithm, called FRP V2. This updated algorithm is based on the previous one, with a similar nighttime algorithm, but includes improved thermal fire detection over daytime products. Daytime detection is performed using a mixed thermal band. The S7 brightness temperature is considered by default for all pixels. In the event of saturation, the F1 channel is used instead for the saturated pixel, and all pixels around it in a 11 x 11 pixels window that either have a S7 brightness temperature above 300 K, or a brightness temperature difference between S7 and S8 higher than 10 K. AF detection during nighttime remains similar to that of the FRP V1 algorithm and uses the F1 measurements. The FRP V2 algorithm also introduced an alternative fire detection using SWIR channels, however this functionality is not yet part of the validation report.

This report only focuses on measurements obtained from the thermal channels using the FRP V2 algorithm over the months of April, May, and June. First, the fires detected during nighttime are assessed. Then, the same analysis is repeated for daytime fires.

7.2 Validation methodology

Validation of the SLSTR L2 FRP products can be performed using either in-situ data such as airborne measurements or using products from a reference satellite for inter-comparison. Active fires in situ data are unfortunately not frequent enough to validate fire satellite data products on an operational basis. The current comparison methodology uses products from NASA Moderate-Resolution Imaging Spectroradiometer (MODIS) as reference fire data for the intercomparisons.

This present inter-comparison, initially based on previous work from M. Wooster and W. Xu on the FRP Prototype and on the evaluation of SEVIRI fire data, aims to assess two things:

(i) The detection of fires' position and extent in time and space.

(ii) The estimated radiative fire power (FRP) of active fires.

To do so, the SL_2_FRP product from SLSTR-A and SLSTR-B are compared with the operational MODIS MOD14 FRP product from MODIS Terra. This inter-comparison should not be interpreted as a full validation exercise but rather as a check of the consistency of the FRP products derived from the satellites, as ground truth is not available.

The methodology to obtain data fit for comparison purposes is outlined hereafter:

- Once areas of interest have been defined, identify all SL_2_FRP scenes containing active fires;
- Download MODIS MOD14 data with a scene overpass time within ± 6 minutes from that of SLSTR;
- Restrict observations to a scan angle of ±20° or equivalent pixel area of 1.7 km^2 to avoid edge-of-swath data, and to the common area of detection between the two products. The scan angle was decreased from ±30° to limit possible pixel size discrepancies between MODIS and SLSTR data;

- Reproject MODIS pixels on the SLSTR F1 grid. If multiple MODIS active fire pixels (AFP) are present in the same equivalent SLSTR grid cell, their combined FRP is used.

Omissions, commissions, and double detections are then evaluated. A fire is classified as omitted if no SLSTR fire pixel is present in a 7 x 7 pixels window around a MODIS fire pixel. Conversely, a fire is classified as commissioned if no MODIS fire pixel is present in a 7 x 7 pixels window around a SLSTR fire pixel. If SLSTR and MODIS pixels are present within the windows, the fire is classified as double detected.

The FRP analysis is twofold: it is done both at the pixel level, and at the cluster level. A cluster is defined as fires close enough to be interpreted as a single fire event (i.e. the detected fire pixels are next to one another). In both cases, as MODIS FRP data is provided before atmospheric correction, they are atmospherically corrected using the water vapor content estimated by Sentinel 3 as the basis to compute the transmission.

The detected fire clustering is done according to the following procedure: for both sensors, a connected-component labeling using an 8-connectivity is used to label clusters. Then, iteratively, clusters from one satellite having an overlap with clusters from the other are merged to form superclusters, until each supercluster from one satellite only overlaps with a single supercluster from the other. Figure 31 illustrates the process. Finally, superclusters associated with problematic flags (clouds/water/detection/high S7-S8 difference) are removed from the datasets. The remaining matching pairs of SLSTR and MODIS superclusters are used for further analysis regarding FRP estimates.

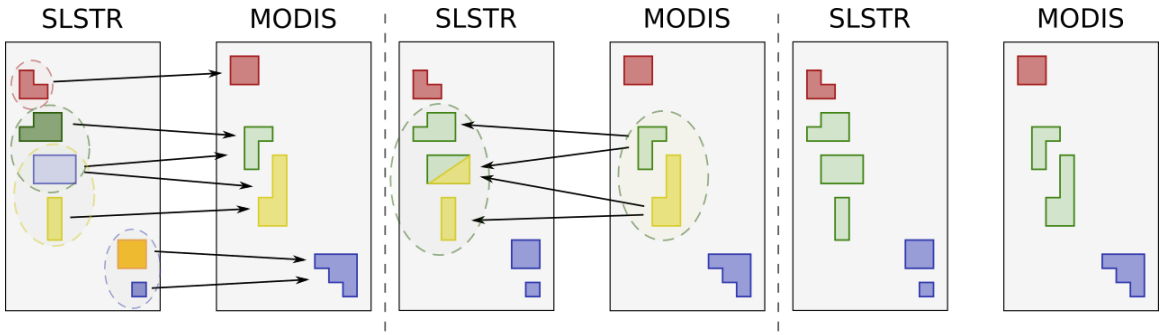

Figure 31: Formation process of the pairs of superclusters depending on AFP detected each satellite. Fire clusters and superclusters are identified by their colors. At the end of the process, pairs of SLSTR and MODIS superclusters share the same color.

Four areas of high fire activity between July 1st and September 30th were selected: western Canada, Europe, Central Africa, and China (see Figure 32). Since the last report, a mean of assessing the FRP estimated from the SWIR bands through cross-comparison with those of the MWIR bands was included.

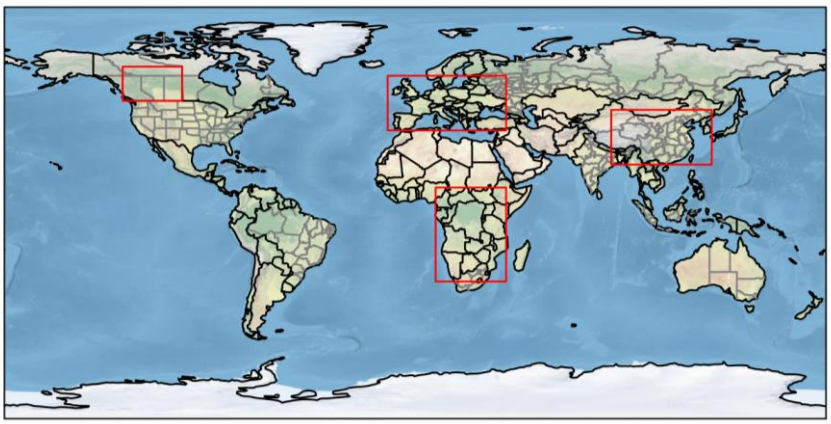

Figure 32: Selected zones for the intercomparison over the July-September 2023 period

7.3 Results

7.3.1 Global distributions of the fires

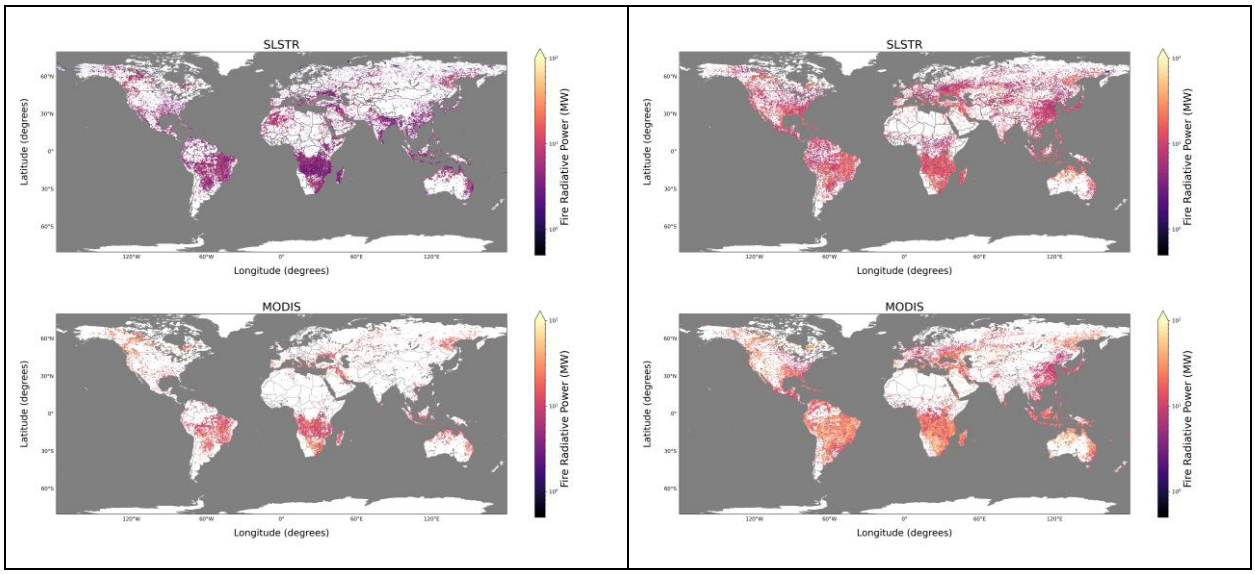

Figure 33: Fires detected by SLSTR and MODIS at nightime (left) and daytime (right).

Figure 33 shows the location and radiative power of fires detected by SLSTR and MODIS during night and daytime. On one hand, SLSTR seems to be detecting more fire than MODIS during nighttime, most of them having a lower intensity, while there are few omissions. On the other hand, during daytime, omissions seem to be much more frequent, especially in the southern hemisphere, with large swathes of Brazil, southern Africa, and Australia presenting MODIS fires when no fire was detected by SLSTR.

7.3.2 Nighttime Fires Validation

7.3.2.1 MWIR fires

Table 10 presents a summary of the intercomparison between active fires detected by SLSTR and MODIS over the July—September 2023 period, as well as past periods. As for previous periods, the data present a significantly larger quantity of commissions (about half of SLSTR-detected fires are commissions) compared to the omissions. Omissions are stable compared to the previous period, during which refinements in the reprojection between MODIS and SLSTR grids were introduced. The FRP distributions of both MODIS and SLSTR clusters are both higher than past periods before April 2023 for the 25th, 50th, and 75th percentile values. While this may be due to the occurrence of more intense fires, it may also be due to the updated clustering values introduced since April.

Table 10: Summary of the intercomparison between nighttime SLSTR and MODIS active fires over the July—September 2023 period. Results from previous 3-months comparisons are included for information purposes.

Variable	Value				
	2023		2022		
	Jul.—Sep.	Apr.—Jun.	Jan.—Mar.	Oct.—Dec.	Jul.—Sep.
Commissions (% of total SLSTR AFP)	54%	49%	56%	55%	62%
Omissions (% of total MODIS AFP)	3%	3%	14%	17%	18%
SLSTR AFP double detec. (% of total SLSTR AFP)	46%	51%	44%	45%	38%
MODIS AFP double detec. (% of total MODIS AFP)	97%	97%	86.0%	83%	82%
Total SLSTR AFP	82,970	19,265	26,911	23,758	32,239
Total MODIS AFP	10,921	3,323	4,048	4,035	4,972
Percentiles 25, 50, 75 of SLSTR clusters FRP (MW)	19, 39, 102	10, 34, 61	11, 19, 35	12, 21, 40	12, 22, 43
Percentiles 25, 50, 75 of MODIS clusters FRP (MW)	10, 25, 72	17, 23, 79	7, 12, 23	8, 14, 30	8, 14, 31
Mean bias of FRP per cluster (MW)	17	-59	7	7	5
Median of FRP scatter per cluster (MW)	9	8	5	6	5

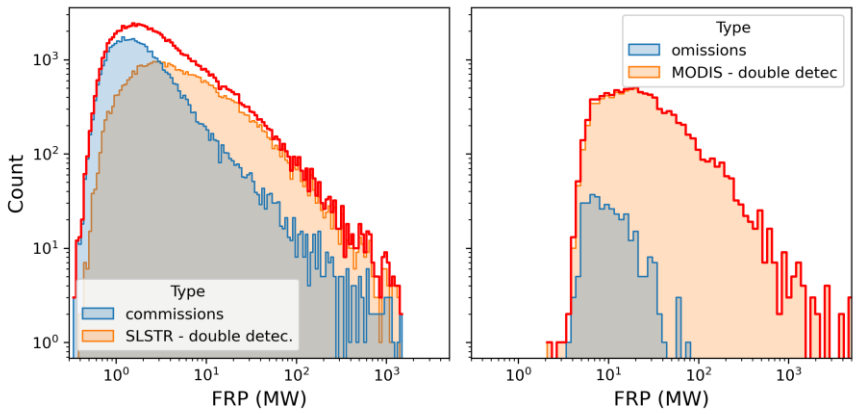

Figure 34: For nighttime: (left) in red, the histogram of all FRP estimated from SLSTR; in blue and orange, a breakdown between commissions and double detections, respectively. (right) in red, the histogram of all FRP estimated from MODIS; in blue and orange, a breakdown between commissions and double detections, respectively.

As visible in Figure 34, a large proportion of the fire pixels SLSTR detects present a very low FRP (< 4 MW). Conversely, almost fire pixel detected by MODIS had a FRP above 4 MW. The distribution of the FRP of

commission pixels confirms that almost all commissions concern fires with very low FRP, highlighting the fact that SLSTR is much more sensitive than MODIS to detect active fires. Omissions, on the other hand, concern fires of very common intensities (~10 MW). Figure 35 shows that there is a good agreement between the FRP of clusters detected by MODIS and those detected by SLSTR. For low FRP values, SLSTR clusters seem to be more intense, which is in line with the lower threshold of SLSTR to detect an AFP: this allows for the detection of larger low-intensity clusters. Overall, the median absolute error between MODIS and SLSTR cluster FRP is 15 MW.

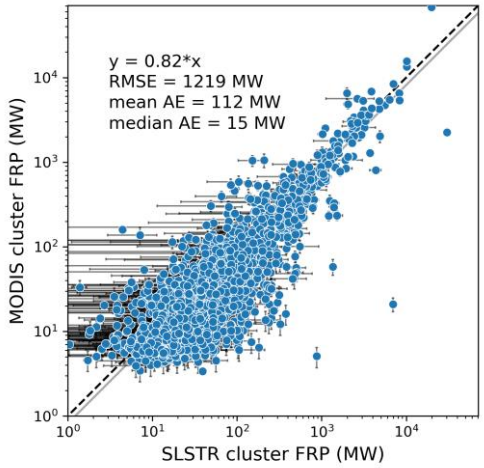

Figure 35: Comparison between the FRP of cluster pairs detected by SLSTR and MODIS during nighttime

7.3.2.2 SWIR fires

The AFP and FRP detected by the SWIR channels are now part of this validation report. Only the FRP value estimated from the SWIR channels is validated, through by cross-comparison with those estimated from the MWIR channels. As SWIR and MWIR channels do not have the same sampling grid (500 m vs 1 km), the validation algorithm is as follow:

1. Reproject the SWIR fires on the MWIR grid using nearest-neighbours;
2. Cluster the SWIR fires and link them to MWIR fires (as done in Figure 31 with SLSTR MWIR and MODIS);
3. Compute the total FRP value of SWIR and MWIR cluster. For MWIR clusters, only take into account the FRP of pixels for which there is an associated SWIR value;
4. Compare estimated MWIR and SWIR cluster FRP.

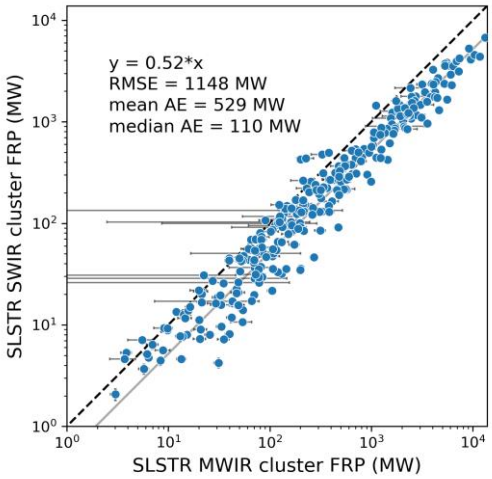

Figure 36: Comparison between the FRP of cluster pairs detected by SLSTR MWIR and SWIR bands during nighttime.

Figure 36 shows that there is a good correlation between the FRP of clusters detected by the MWIR and the SWIR bands over the whole range. However, it appears that there is a difference in the intensity of the cluster FRP estimated by the bands: SWIR cluster FRP is, overall, half the intensity of the MWIR cluster FRP (slope of 0.52). Since for this comparison the extents of MWIR clusters were limited to those of SWIR cluster, it appears that the SWIR bands lead to lower FRP for the same fire events.

7.3.3 Daytime Fires Validation

Table 11 presents a summary of the intercomparison between active fires detected by SLSTR and MODIS over the July—September 2023 period, as well as past periods. The proportion of commissioned fire pixel is in line with previous periods, while the proportion of omissions is in line with the April—June 2023 period. This difference in proportion between before and after April 2023 corresponds to the introduction of the improvements in the MODIS-SLSTR grid matching improvements. The FRP distributions of both MODIS and SLSTR clusters are higher than past periods before April 2023 for the 25th, 50th, and 75th percentile values. While this may be due to the occurrence of more intense fires, it may once again be due to the updated clustering values introduced since April.

Table 11: Summary of the intercomparison between daytime SLSTR and MODIS active fires over the July-September 2023 period. Results from previous 3-months comparisons are included for information purposes.

Variable	Value				
	2023			2022	
	Jul.—Sep.	Apr.—Jun.	Jan.—Mar.	Oct.—Dec.	Jul.—Sep.
Commissions (% of total SLSTR AFP)	43%	31%	27%	48%	49%
Omissions (% of total MODIS AFP)	33%	27%	42%	46%	49%
SLSTR AFP double detec. (% of total SLSTR AFP)	57%	69%	73%	52%	51%
MODIS AFP double detec. (% of total MODIS AFP)	67%	73%	58%	54%	51%
Total SLSTR AFP	37,754	22,069	16,257	11,163	15,667
Total MODIS AFP	20,458	10,930	14,946	8,114	11,565
Percentiles 25, 50, 75 of SLSTR clusters FRP (MW)	18, 36, 86	17, 37, 90	15, 28, 51	17, 27, 52	16, 27, 54
Percentiles 25, 50, 75 of MODIS clusters FRP (MW)	15, 32, 82	19, 35, 91	12, 22, 46	13, 22, 43	14, 23, 50
Mean bias of FRP per cluster (MW)	-9	-13	6	4	5
Median of FRP scatter per cluster (MW)	3	3	4	4	3

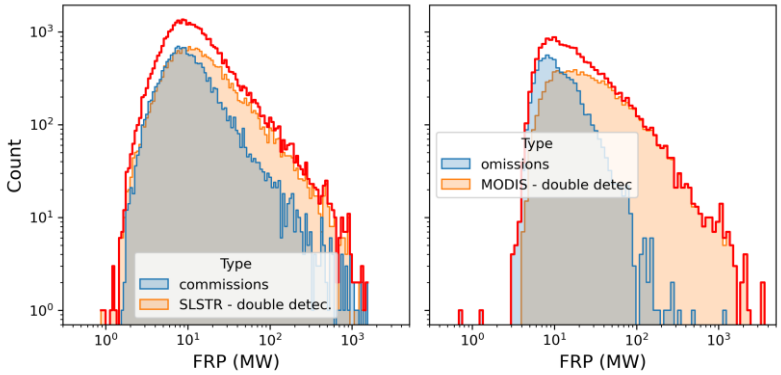

Figure 37: From left to right, for daytime: histograms of the FRP of fires detected by SLSTR and MODIS, histogram of the FRP of commissions, histogram of the FRP of omissions.

Figure 37: From left to right, for daytime: histograms of the FRP of fires detected by SLSTR and MODIS, histogram of the FRP of commissions, histogram of the FRP of omissions.Figure 37 is the equivalent to Figure 34, but for daytime. The same patterns are observed: a large proportion of the fire pixels SLSTR detects present a very low FRP (< 4 MW), unlike MODIS. In a similar fashion as for nighttime, commissions almost exclusively present very low FRP values, while omissions are, for the most part, average-intensity fires.

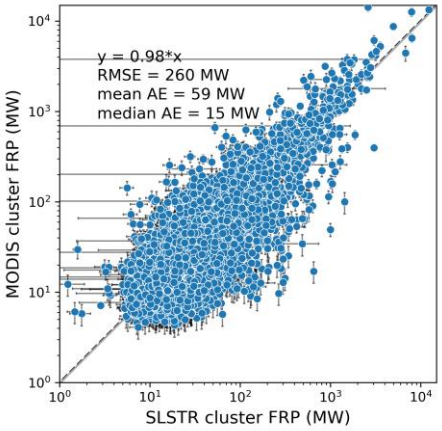

Figure 38: Comparison between the FRP of cluster pairs detected by SLSTR and MODIS during daytime.

7.3.4 Biome influence on active fire detection

The present section consists in a preliminary study on the biome influence over errors of commission and omission. The biome corresponding to each fire is determined using the Global Land Cover 2000 data. This per-biome analysis may help identify biome-dependent behaviours concerning active fire detection. For each biome, over nighttime and daytime, the absolute numbers of commissions and omissions as well as the relative numbers (with regards to the total number of SLSTR and MODIS AFP for commissions and omissions, respectively) are evaluated over the July—September 2023 period.

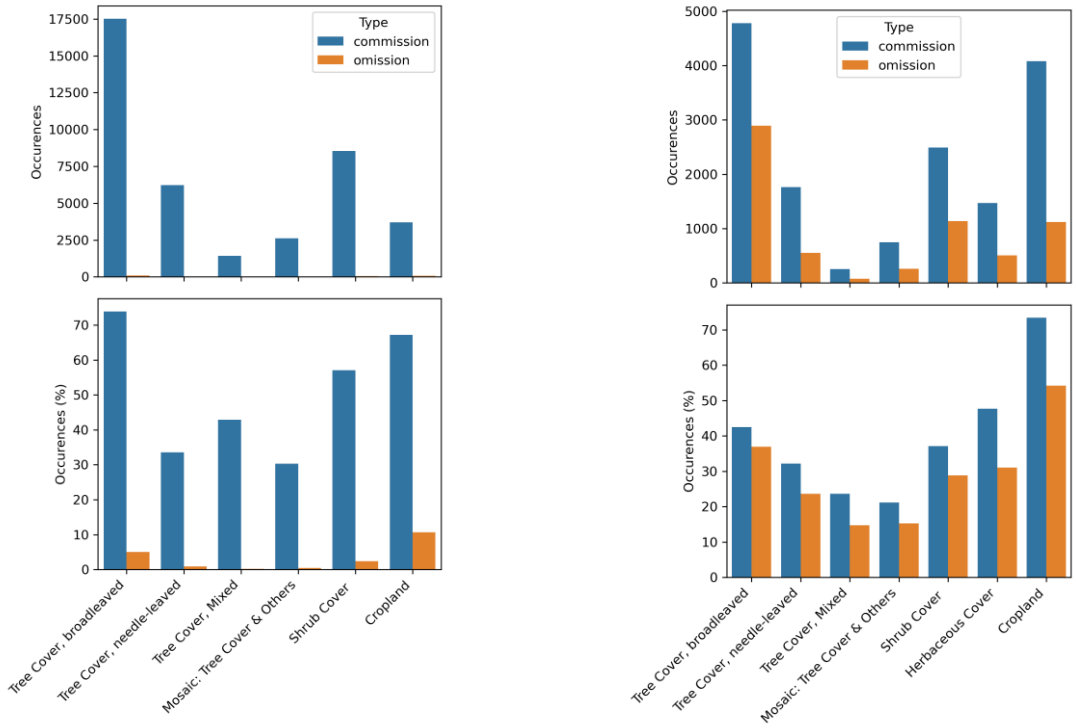

Figure 39: Occurrences of commissions and omissions of active fire pixels per biome. On the left, nighttime; on the right, daytime.

Figure 39 shows the absolute (top) and relative number (bottom) of commissions and omissions. For clarity purposes, similar biomes were aggregated together, while some were rejected from the analysis. For both nighttime and daytime, the percentage of commissions from Treed Needle-leaved Evergreen is lower than the average, with values around 30% in both cases, versus 54% and 43% commissions on average for nighttime and daytime, respectively. As with the previous period, the Treed Broadleaved biomes have higher than average percentages of commissions (more than 70% for nighttime) with non-negligible quantities of active fire detections. For daytime, croplands also present a very high number of commissions, which might correspond to low intensity agricultural burnings.

7.4 Conclusion

This performance report seems to confirm that the accuracy improvements of the geographic locations of fires in the FRP monitoring algorithm put in place for the last report have led to a reduction in the number of commissions and omissions compared to previous periods. This period, as the last one, showed that the active fires detected by the satellites were much more in line, with increased numbers of double detections.

Overall, in line with previous reports, it appears that for both nighttime and daytime products, much more AFP are detected by SLSTR than MODIS. Indeed, SLSTR's FRP threshold to detect active fires is much lower than that of MODIS (<1 MW vs ~3 MW), leading to a very high number of low intensity commissioned fires.

For most active fire clusters, trends are coherent with past periods, with good agreement between SLSTR and MODIS clusters' FRP. The reduction in maximum scan angle from 30° to 20° may have contributed to the better relationship between SLSTR and MODIS cluster, as possible pixel size discrepancy was more limited. Overall, for both daytime and nighttime, there seem to be a linear relationship between MODIS and SLSTR cluster FRP, and a median absolute error of 15 MW.

The analysis of the FRP estimated from the SWIR bands showed that while there is indeed a linear relationship between the SWIR cluster and their SWIR counterparts, the relation is not 1:1. Presently, it appears that cluster FRP estimated from the SWIR bands is about half of that estimated from the MWIR bands (factor of 0.52). Further analysis of the SWIR FRP values and distribution, as well as fire location, is needed.

The results of the per-biome analysis seem to confirm behavioural differences between Broadleaved and Needle-leaved biomes: although both present high quantities of fire detections, as would be expected from forests, the former are much more prone to commissions than the latter (>70% versus ~30% and ~40% versus ~30%, for nighttime and daytime, respectively). Shrublands and Croplands presented a very high quantity of commissions at nighttime, and Croplands still presented a very high number of commissions during daytime (>70%). This may be explained by the lower detection threshold of SLSTR (~1 MW), which may detect smaller agricultural fires

8 Appendix A

All Data Quality Reports, as well as past years Data Quality Reports and Annual Performance Reports, are available on dedicated pages in Sentinel Online website, at:

- https://sentinel.esa.int/web/sentinel/technical-guides/sentinel-2-msi/data-quality-reports
- https://sentinel.esa.int/web/sentinel/technical-guides/sentinel-3-olci/data-quality-reports
- https://sentinel.esa.int/web/sentinel/technical-guides/sentinel-3-slstr/data-quality-reports
- OPT Annual Performance Report Year 2022 (PDF document)

End of document